Solitons in cell membranes

Pradip Das and W. H. Schwarz
Institute for Biophysical Research on Macromolecular Assemblies, The Johns Hopkins University, Baltimore, Maryland 21218
(Received 28 June 1993; revised manuscript received 4 November 1994)

Using a two-dimensional smectic liquid crystal model, we have shown the plausibility of electrical solitary wave propagation along a bimolecular leaflet such as the cell membrane of a nerve axon which consists of chiral, lipid building blocks. Our model is a head-to-tail correlated ferroelectric, chiral Sm-C^* liquid crystal, which is a unique class of substances that combines the electric polarization and anisotropy of ferroelectric crystals with the hydrodynamic properties of liquids. Polar Sm-A models can also be used with the same results. In addition to the usual transverse ferroelectricity, characteristic of the Sm-C^* liquid crystal, the head-to-tail correlation ensures a longitudinal ferroelectricity component. The electric polarization due to the latter can couple to the transmembrane electric field resulting from the ionic imbalance between the two sides of the membrane—a mechanism detailed in the so-called Hodgkin-Huxley set of partial differential equations for the propagation of the action potential. We obtain a Landau–de Gennes–like free energy, which is the sum of elastic, fluctuation, and polarization terms, together with a ferroelectric term showing a direct coupling between the electric field and the mechanical deformation variable. Minimizing and equating to a viscous damping term leads to an equation similar to one equation of the Fitzhugh-Nagumo coupled set of partial differential equations, which is a simplified version of the Hodgkin-Huxley equations. The other equation of the set resembles an equation derived from the Nernst-Planck equation, which describes transmembrane ion transport and hence provides a mechanism for transmembrane potential variation. A more complete calculation of the velocity of the asymptotic wave form shows a lower wave speed than the estimate of Nagumo *et al.* The piezoelectric properties of the phase compete with its curvature elasticity to produce the soliton lattice of the cell membrane, which consists of juxtaposed regions of opposite tilt orientations. The propagation of the solitary wave requires a switching electric field, which is the form for the action potential and which moves the polarized domains by ferroelectric switching.

PACS number(s): 87.22.−q, 61.30.Cz, 77.80.Fm

I. INTRODUCTION

The nerve axon membrane has been thoroughly studied since the seminal work of Hodgkin and Huxley [1], who hypothesized that the dependence of sodium and potassium conductances on the membrane potential could arise from the effect of the electric field on the distribution or orientation of molecules with a charge or dipole moment. The structure of the membrane generally accepted at present is due to Singer and Nicolson [2]. This fluid mosaic model of the cell membrane is a two-dimensional (2D) smectic liquid crystal composed of a phospholipid bilayer. Imbedded in this bimolecular leaflet are small patches of transport proteins which allow the transmission of ions [2,3].

The propagation of action potentials in cell membranes, muscle, retinal photoreceptors, and myelin are well known. All of these organized systems possess a lamellar or smectic structure. Cladis and Van Saarloos [4] attribute ferroelectric properties to these structures, arising out of the occurrence of chiral building blocks.

Because of the variety of possible short- and long-range ordering, thermotropic smectic liquid crystals have a great diversity of forms [5]. The Sm-A phase is uniaxial and possesses the orientational order of the nematics plus a 1D mass density modulation which is in the same direction as the "nematic" director. The Sm-C phase is biaxial and is characterized by the noncoincidence of the nematic director with the density modulation. The difference between the Sm-C and Sm-A phases is the angle of tilt of the molecules in the former (see Fig. 1). Both Sm-A and Sm-C phases have "liquid" layers, i.e., there is no positional correlation among the molecules in any single layer, just as in a liquid. Other smectic phases have "solid" layers and are more difficult to characterize. We exclude

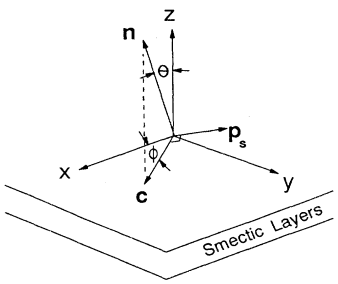

FIG. 1. Sketch of the ferroelectric liquid crystal geometry. The smectic-C^* phase has layering along the z direction. The molecular director $\mathbf{n}$ is tilted from the layer normal by an angle θ and the spontaneous polarization $\mathbf{p}_s$ is along the direction defined by $\mathbf{i}_z \times \mathbf{n}$. $\mathbf{c}$ represents the c director, which lies in the smectic plane and is perpendicular to $\mathbf{p}_s$.

them from further discussion and restrict ourselves to the liquid layer smectics. Also, we note that many of the characteristics of the thermotropics are displayed by the lyotropics.

Under the resting condition, the cylindrical nerve axon maintains a constant potential difference across its surface membrane. If a stimulus in the form of a brief outward current pulse of millisecond duration is applied through a stimulating electrode touching the membrane, the resulting potential change depends on the stimulus. A stimulus below a threshold level causes a membrane potential change, which is below ~ 10 mV, and decays fast. With the application of a transthreshold stimulus, the recorded potential curve increases abruptly in amplitude to form the triangular, ~ 100-mV-high (about 1–2 ms duration), wave form called an action potential. This electric pulse signal is transmitted along an unmyelinated animal nerve axon at constant conduction velocity with neither attenuation nor distortion, regardless of the distance traveled. The signal is characterized by an asymptotic value of the height (~ 0.1 V) and width (~ 2 ms). Any initial disturbance imparted to the excitable nerve membrane can be (i) attenuated, if the signal height is above the asymptotic value; (ii) amplified, if the signal height is below the asymptotic value but above a certain threshold value; and (iii) eliminated, if the signal height is below the threshold value [6,7].

The set of partial differential equations developed by Hodgkin and Huxley to describe the propagation of the action potential was examined by Fitzhugh [6] and Nagumo, Arimoto, and Yoshizawa [7]. The latter authors showed that the propagation of asymptotic wave forms is described by a coupled set of differential equations. Wang [8] considered field-induced, mechanical solitary waves in nematic liquid crystals and showed their relationship to a simple case of the Fitzhugh-Nagumo (FN) coupled set of equations. Using a 2D smectic liquid crystal model, Chao and White [9] predicted the existence of mechanical solitons (orientational waves) in the cell membranes under a transmembrane electric field. They were motivated by the prediction of Fergason and Brown [10] that a variety of solitons, e.g., splay-bend waves, can propagate along the 2D smectic liquid crystalline plasma membranes of cells and through the cytoskeletonal fluid, which is a nematic liquid crystal, thereby acting as a method of information transfer. Zhu [11] was also motivated by the Fergason-Brown prediction and experimentally demonstrated that mechanical solitons can propagate in nematics under shear and estimated the speed of their propagation.

The fundamental question that we are addressing here is whether these propagating action potentials are indeed electrical solitons or not. We show that equations similar to the FN coupled set is derivable from the ferroelectric smectic liquid crystal model of the cell membrane and that the solitary wave is the result of ferroelectric liquid crystal switching plus the cable variation of the electric field. We derive an expression for the conduction velocity in terms of the mechanical (e.g., anisotropic elastic constants and viscometric coefficients) and electrical (e.g., membrane capacity) constants of the material constituting the membrane, molecular parameters such as membrane thickness, and macroscopic parameters such as axon radius.

II. ELECTRIC POLARIZATION IN BIOLOGICAL MEMBRANES

Lipid extracts from a variety of cell membranes exhibit strong thermal behavior at ambient temperatures as evidenced by the observation of the undulations of the surface [12]. However, thermally induced phase changes are not usually important in biological systems since most living organisms function at a fairly constant temperature. Still, phase changes can be induced by alterations in chemical composition of the membrane as well as by certain environmental variations, such as changes in pH, ionic strength, and the electric field across a membrane [13].

Keeping in mind the liquid crystal analogy of the cell membrane, one would naturally look for the source of spontaneous electric polarization, which can couple to the electric field and result in rapid wave propagation. Fast-traveling, electrically induced solitons are known in ferroelectric Sm-C^* phases [14]. In a tilted smectic phase such as Sm-C^*, which is built of chiral building blocks, the dipoles add up to give a spontaneous electric polarization $\mathbf{p}_s$, a vector which is perpendicular to the plane formed by the layer normal and the molecular direction (see Fig. 1).

The free energy of this phase in the presence of the electric field is written as [4]

$$F=\int dx \left[\frac{K\theta^2}{2}\left(\frac{d\phi}{dx}+q_0\right)^2 - \frac{\varepsilon_a\theta^2}{8\pi}E^2\sin^2\phi - p_s\theta E\cos\phi \right] .$$

We adopt the usual convention that in a right-handed coordinate system $q_0 \equiv 2\pi/T > 0$ is a right-handed helix, where T is the pitch of the helix, ε_a is the dielectric anisotropy, and $K \equiv K_{11}=K_{22}=K_{33}$, where the K_{jj} are the elastic moduli (the one-constant assumption). θ is the Sm-C^* tilt angle indicated in Fig. 1. $\theta=0$ for Sm-A phases; $\mathbf{c}$ is the c director, which is the projection of the molecular director on the x-y plane; $\mathbf{p}_s(\perp\mathbf{c})$ is the electric polarization vector and p_s is its magnitude; $\mathbf{p}_s=(\cos\phi(z),\sin\phi(z),0)$; and $\mathbf{E}=E(0,1,0)$.

The soliton equation is obtained by minimizing the bracketed quantities of the free-energy expression and equating the result to the viscous damping term $\gamma\theta^2\partial\phi/\partial t$:

$$K\theta^2\frac{\partial^2\phi}{\partial x^2}+\frac{\varepsilon_a\theta^2}{4\pi}E^2\cos\phi\sin\phi-\theta p_s E\sin\phi=\gamma\theta^2\frac{\partial\phi}{\partial t} . \quad (1)$$

Extensive numerical solutions for this equation have been reported [14].

In order to obtain a ferroelectric liquid phase, the molecules should be chiral with a transverse dipole moment [15]. Note that it is not possible to superimpose the molecule on its mirror image and that cholesteric and

smectic-A phases cannot support this type of transverse ferroelectricity.

There is, however, another type of ferroelectric phase, e.g., the longitudinal type. This is exemplified by bilayer smectics. At a first glance, these smectics can belong to either of the categories smectic A or smectic C and also in the undulated or rippled phase. Cell membranes are lipid bilayers of this type and exhibit the full gamut of variations [12]: Sm-A, Sm-C, rippled, etc. Lipid molecules are typical amphiphiles with a large polar head group and a nonpolar hydrocarbon chain. Such phases have a spontaneous electric polarization which is along the layer normal. Cell membranes are very thin ($\sim$50–100 Å thick and virtually 2D) and subject to thermal fluctuations, described by long-wavelength displacements $u(x,y,z,t)$. The quantity u varies slowly and its spatial derivatives, which express the layer deformations, are small ($\langle u(x,y,z)\rangle=0$ and $|u(x,y,z)| \ll 1$). To second order, the components or direction cosines of the layer normal $\mathbf{n}$ are given by [16]

$$\mathbf{n}=\left\{-\frac{\partial u}{\partial x}\left[1+\frac{\partial u}{\partial z}\right],-\frac{\partial u}{\partial y}\left[1+\frac{\partial u}{\partial z}\right],1-\frac{1}{2}\left[\left[\frac{\partial u}{\partial x}\right]^2+\left[\frac{\partial u}{\partial y}\right]^2\right]\right\}.$$

$\partial u/\partial z=0$ for 2D cell membranes. In the absence of an electric field, the total free energy for the 2D cell membrane is given by [17]

$$F=\int dx\,dy\,dz\left\{\frac{1}{2}K_{11}\left[\frac{\partial^2 u}{\partial x^2}+\frac{\partial^2 u}{\partial y^2}\right]^2+\frac{\sigma}{d}\left[\left[\frac{\partial u}{\partial x}\right]^2+\left[\frac{\partial u}{\partial y}\right]^2\right]\right\},$$

where σ is the interfacial surface energy, d is the membrane thickness, and K_{11} is the splay elastic constant. The terms in parentheses take account of the splay bending of the layer and the surface energy due to the increase in the interfacial area respectively.

Now we do the following: (a) carry out the z integration to give $\int dz=d$ and (b) consider an *axisymmetric* membrane as is normally found in living systems. Switching to cylindrical coordinates (r,α,x) (see Fig. 2), we find, for smectic-A symmetry,

$$F=\int r\,dr\,d\alpha\,dx\left\{\frac{1}{2}K_{11}\left[\left[\frac{1}{r}\frac{\partial}{\partial r}r\frac{\partial u}{\partial r}+\frac{1}{r^2}\frac{\partial^2 u}{\partial \alpha^2}+\frac{\partial^2 u}{\partial x^2}\right]\right]^2+\frac{\sigma}{d}\left[\left[\frac{\partial u}{\partial x}\right]^2+\frac{1}{r^2}\left[\frac{\partial u}{\partial \alpha}\right]^2\right]\right\}. \quad (2)$$

Since the membrane is very thin ($\sim$75 Å), we take $\partial u/\partial r=0$. This is equivalent to the assumption that $\partial u/\partial z=0$ in Cartesian coordinates, as already noted [17]. Also, axisymmetry implies that $\partial u/\partial\alpha=0$. Thus we obtain

$$F=\pi(R_o^2-R_i^2)\int\left[\frac{K_{11}}{2}\left[\frac{\partial^2 u}{\partial x^2}\right]^2+\frac{\sigma}{d}\left[\frac{\partial u}{\partial x}\right]^2\right]dx\,, \quad (3)$$

where R_o and R_i are the outer and inner radii, respectively. This is now a 1D problem. Referring to Fig. 3 we write

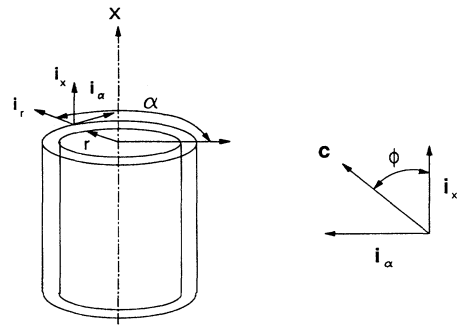

FIG. 2. Definition of the coordinate system used to describe the smectic layer. The coordinate system is cylindrical, with the x axis coinciding with the axis of the cylinder. The r direction is everywhere parallel to the normal to the smectic layer. The angle ϕ measures the rotation of the c director with respect to the x axis as shown in the right-hand part of the figure.

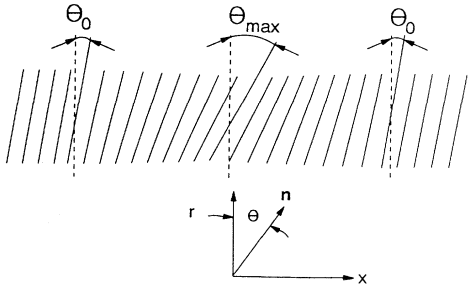

FIG. 3. Splay wave in a 1D membrane. θ_0 is the equilibrium-tilt angle of the local molecular director with respect to the layer normal, i.e., the r direction. θ_{max} is the maximum tilt at the peak of the splay wave.

$$n_x=-\frac{\partial u}{\partial x}=\sin\theta(x,t),\quad n_\alpha=0,\quad n_r=\cos\theta(x,t)\ . \tag{4}$$

Using these results in Eq. (3), one obtains

$$F=\pi R K_b\int dx\left[\left[\frac{\partial\theta}{\partial x}\right]^2+\frac{4\sigma}{K_b}\left[\theta^2-\frac{\theta^4}{3}\right]\right], \tag{5}$$

where the approximations [18]

$$\sin\theta\approx\theta,\quad \cos2\theta\approx1-\frac{(2\theta)^2}{2!}+\frac{(2\theta)^4}{4!}$$

have been used. Further,

$$R_o^2-R_i^2=(R_o+R_i)(R_o-R_i)=2Rd\ ,$$

where R is the mean radius. Also,

$$K_b\equiv K_{11}d\ .$$

K_b, known as the bending constant, determines the amplitude of thermal fluctuations of the membrane [17]. Consequently, observation of the latter gives a method of determining K_b. Experimentally, Brochard and Lennon [19] found $K_b\sim(1-2)\times10^{-19}$ J. From the elastic theory of liquid crystals [20], we know that K_{11}, the splay elastic constant, $\approx6\times10^{-7}$ dyn. Also, the membrane thickness $d\approx75$ Å. Hence K_b (calculated) $\approx4.5\times10^{-13}$ ergs$=4.5\times10^{-20}$ J. The agreement seems rather good. Equations (2)–(5) strictly hold for a bilayer membrane having a smectic-A symmetry.

For smectic-C symmetry, we need to start from the form for the Sm-C elastic energy density [21]

$$\begin{aligned}F'=&\frac{1}{2}K^0\left[\left[\frac{\partial\xi_1}{\partial z}\right]^2+\left[\frac{\partial\xi_2}{\partial z}\right]^2\right]+\frac{1}{2}K'\left[\frac{\partial\xi_1}{\partial x}+\frac{\partial\xi_2}{\partial y}\right]^2\\&+\frac{1}{2}K''\left[\frac{\partial\xi_1}{\partial y}-\frac{\partial\xi_2}{\partial x}\right]^2\\&+K'''\left[\xi_1\frac{\partial\xi_2}{\partial z}-\xi_2\frac{\partial\xi_1}{\partial z}\right]\left[\frac{\partial\xi_1}{\partial y}-\frac{\partial\xi_2}{\partial x}\right],\end{aligned} \tag{6}$$

where the two-component, tilt-vector order parameter $\xi=(\xi_1,\xi_2)$ is given by

$$\begin{aligned}\xi_1&=n_xn_z=\sin\theta\cos\theta\cos\phi\ ,\\ \xi_2&=n_yn_z=\sin\theta\cos\theta\sin\phi\end{aligned} \tag{7}$$

and K^0, K', K'', and K''' are the Sm-C elastic moduli [21]. We assume θ to be small, so that

$$\xi_1\approx\theta\cos\phi\approx n_x,\quad \xi_2\approx\theta\sin\phi\approx n_y\ .$$

Thus

$$\begin{aligned}F'\approx&\frac{1}{2}K^0\left[\left[\frac{\partial n_x}{\partial z}\right]^2+\left[\frac{\partial n_y}{\partial z}\right]^2\right]+\frac{1}{2}K'\left[\frac{\partial n_x}{\partial x}+\frac{\partial n_y}{\partial y}\right]^2\\&+\frac{1}{2}K''\left[\frac{\partial n_x}{\partial y}-\frac{\partial n_y}{\partial x}\right]^2\\&+K'''\left[n_x\frac{\partial n_y}{\partial z}-n_y\frac{\partial n_x}{\partial z}\right]\left[\frac{\partial n_x}{\partial y}-\frac{\partial n_y}{\partial x}\right].\end{aligned}$$

Ignoring the z dependence of θ and ϕ, which is justifiable because of the thinness of the layer, and using the one-constant approximation ($K'=K''=K$), we obtain

$$F'\approx\tfrac{1}{2}K[(\nabla\theta)^2+\theta^2(\nabla\phi)^2]+4\sigma\left[\theta^2-\frac{\theta^4}{3}\right], \tag{8}$$

which also includes the interfacial energy term obtained from Eq. (5).

The first two terms in Eq. (8) are considered to be the fluctuation terms and the third one is the elastic term. We need higher-order elastic terms in Eq. (8) to take into account the fact that the smectic layer is stacked in the form of a cylinder in the nerve axon. For a cylindrical smectic-A thin layer, the elastic energy density contribution is $K_{11}/2R^2$, where K_{11} is the splay elastic constant and R is the mean radius of the cylindrical membrane. The cylindrical smectic-C elastic layer energy, of which the smectic-A result given above ($K_{11}/2R^2$) is a special case, is obtained from Fig. 2.

We write, following Carlsson, Stewart, and Leslie [22],

$$w_{\text{layer}}^{(\phi)}=\frac{1}{2R^2}(A_{12}\sin^4\phi+A_{21}\cos^4\phi-2A_{11}\sin^2\phi\cos^2\phi)\ ,$$

where $w_{\text{layer}}^{(\phi)}$ is the thin-layer energy, ϕ is the azimuthal angle, and the A's are elastic constants. Carlsson, Stewart, and Leslie [22] expanded A_{21} in powers of the tilt angle θ, retaining only the first even power term in θ. In order to examine the relevance of a higher-order approximation, we add the fourth-power terms

$$\begin{aligned}A_{21}&=K_{11}+\overline{A}_{21}\theta^2+B_{21}\theta^4\ ,\\ A_{12}&=K_{11}+\overline{A}_{12}\theta^2+B_{12}\theta^4\ ,\\ A_{11}&=-K_{11}+\overline{A}_{11}\theta^2+B_{11}\theta^4\ .\end{aligned} \tag{9}$$

Also, the following inequalities, which now include B terms, must be valid [22]:

$$\begin{aligned}&K_{11}>0\ ,\\ &(\overline{A}_{12}+\overline{A}_{21}+2\overline{A}_{11})+(B_{12}+B_{21}+2B_{11})\theta^2>0\ .\end{aligned} \tag{10}$$

Only even powers of θ are allowed because the energy is unchanged on the inversion $\theta\rightarrow-\theta$. Now

$$\begin{aligned}w_{\text{layer}}^{(\phi)}=&\frac{K_{11}}{2R^2}+\frac{1}{2R^2}\{[(\overline{A}_{12}+\overline{A}_{11})\sin^4\phi\\&+(\overline{A}_{21}+\overline{A}_{11})\cos^4\phi]\theta^2\\&+[(B_{12}+B_{11})\sin^4\phi\\&+(B_{21}+B_{11})\cos^4\phi]\theta^4\}\ .\end{aligned} \tag{11}$$

Minimizing with respect to ϕ, one finds

$$\begin{aligned}\theta\sin\phi\cos\phi\{&[(\overline{A}_{12}+\overline{A}_{11})\sin^2\phi-(\overline{A}_{21}+\overline{A}_{11})\cos^2\phi]\\&+[(B_{12}+B_{11})\sin^2\phi-(B_{21}+B_{11})\cos^2\phi]\theta^2\}=0\ .\end{aligned}$$

The form of the energy in Eq. (11) implies that the stable configuration ϕ_0 of the c director will depend on the signs of $\overline{A}_{ij}$ and B_{ij} and we need to distinguish three cases: case 1,

$$(\bar{A}_{12}+\bar{A}_{11})+(B_{12}+B_{11})\theta^2>0\ ,$$

$$\phi_0=0,\pi$$

$$(\bar{A}_{21}+\bar{A}_{11})+(B_{21}+B_{11})\theta^2<0\ ,$$

case 2,

$$(\bar{A}_{12}+\bar{A}_{11})+(B_{12}+B_{11})\theta^2<0\ ,$$

$$\phi_0=\frac{\pi}{2},\frac{3\pi}{2}$$

$$(\bar{A}_{21}+\bar{A}_{11})+(B_{21}+B_{11})\theta^2>0\ ,$$

and case 3,

$$(\bar{A}_{12}+\bar{A}_{11})+(B_{12}+B_{11})\theta^2>0\ ,$$

$$(\bar{A}_{21}+\bar{A}_{11})+(B_{21}+B_{11})\theta^2>0\ .$$

Hence

$$\tan^2\phi_0=\frac{(\bar{A}_{21}+\bar{A}_{11})+(B_{21}+B_{11})\theta^2}{(\bar{A}_{12}+\bar{A}_{11})+(B_{12}+B_{11})\theta^2}\ .$$

A possible case 4 with

$$(\bar{A}_{12}+\bar{A}_{11})+(B_{12}+B_{11})\theta^2<0\ ,$$

$$(\bar{A}_{21}+\bar{A}_{11})+(B_{21}+B_{11})\theta^2<0$$

is not allowed because of the second inequality in Eq. (10).

Thus, for case 1

$$w_{\text{layer}}=\frac{K_{11}}{2R^2}+\frac{1}{2R^2}[(\bar{A}_{21}+\bar{A}_{11})\theta^2+(B_{21}+B_{11})\theta^4]\ ,$$

for case 2

$$w_{\text{layer}}=\frac{K_{11}}{2R^2}+\frac{1}{2R^2}[(\bar{A}_{12}+\bar{A}_{11})\theta^2+(B_{12}+B_{11})\theta^4]\ ,$$

and for case 3

$$w_{\text{layer}}=\frac{K_{11}}{2R^2}+\frac{\theta^2}{2R^2}\frac{[(\bar{A}_{12}+\bar{A}_{11})+(B_{12}+B_{11})\theta^2][(\bar{A}_{21}+\bar{A}_{11})+(B_{21}+B_{11})\theta^2]}{(\bar{A}_{12}+\bar{A}_{21}+2\bar{A}_{11})+(B_{12}+B_{21}+2B_{11})\theta^2}$$

$$=\frac{K_{11}}{2R^2}+\frac{\theta^2}{2R^2}\{(\bar{A}_{12}+\bar{A}_{21})(\bar{A}_{21}+\bar{A}_{11})+\theta^2[(\bar{A}_{12}+\bar{A}_{11})(B_{21}+B_{11})+(\bar{A}_{21}+\bar{A}_{11})(B_{12}+B_{11})]\}$$

$$\times\frac{1}{(\bar{A}_{12}+\bar{A}_{21}+2\bar{A}_{11})}\left\{1-\left[\frac{B_{12}+B_{21}+2B_{11}}{\bar{A}_{12}+\bar{A}_{21}+2\bar{A}_{11}}\right]\theta^2+O(\theta^4)\right\}$$

$$\approx\frac{K_{11}}{2R^2}+\frac{1}{2R^2}[A\theta^2+B\theta^4+O(\theta^6)]\ ,$$

where

$$A\equiv\frac{(\bar{A}_{12}+\bar{A}_{11})(\bar{A}_{21}+\bar{A}_{11})}{(\bar{A}_{12}+\bar{A}_{21}+2\bar{A}_{11})}$$

and

$$B\equiv\frac{\left\{(\bar{A}_{12}+\bar{A}_{11})(B_{21}+B_{11})+(\bar{A}_{21}+\bar{A}_{11})(B_{12}+B_{11})-\dfrac{(B_{12}+B_{21}+2B_{11})(\bar{A}_{12}+\bar{A}_{11})(\bar{A}_{21}+\bar{A}_{11})}{(\bar{A}_{12}+\bar{A}_{21}+2\bar{A}_{11})}\right\}}{(\bar{A}_{12}+\bar{A}_{21}+2\bar{A}_{11})}\ .$$

The experimental determination of the A elastic coefficients has been discussed by Carlsson, Stewart, and Leslie [23]. We will present a similar discussion of the B constants in a later section.

III. POLARIZATION EFFECTS

Both the hydrophilic head groups and the hydrophobic hydrocarbon chains of the lipid bilayers are highly anisotropic structures. The mesomorphic states of the fluid membrane [see Fig. 4(a)] are conveniently described by the de Gennes stretching vector $\mathbf{J}$ [24]: $\mathbf{J}=\mathbf{J}_0\rho(\mathbf{J})$, with $\mathbf{J}_0=\mathbf{J}_h+\mathbf{J}_p$, where $\mathbf{J}_h$ and $\mathbf{J}_p$ define the average orientations of the hydrocarbon chains and polar head groups, respectively. Their absolute values measure the average lengths of the hydrocarbon chains and the polar head groups. $\rho(\mathbf{J})$ represents the lateral density of monomeric units in the lipid for the stretching vector $\mathbf{J}$. A spontaneous electric polarization may be associated with the stretching vector $\mathbf{p}=\langle\mathbf{X}\rangle\mathbf{J}$, where $\langle\mathbf{X}\rangle$ is a tensor averaged over the fast rotational tumbling motion of the lipid molecules. A residual electric polarization in the direc-

tion of the molecular rotational axis is expected. In tilted phases, a component $\hat{\mathbf{p}}_s$ of the polarization parallel to the plane of the membrane and in the direction of the tilt arises [see Figs. 4(a)–4(c)]. In addition, there is a longitudinal component $\mathbf{p}_r$ along the layer normal. A phenomenological expression for this net longitudinal polarization $\mathbf{p}_r$ of a curved bilayer membrane was proposed by Petrov [26]:

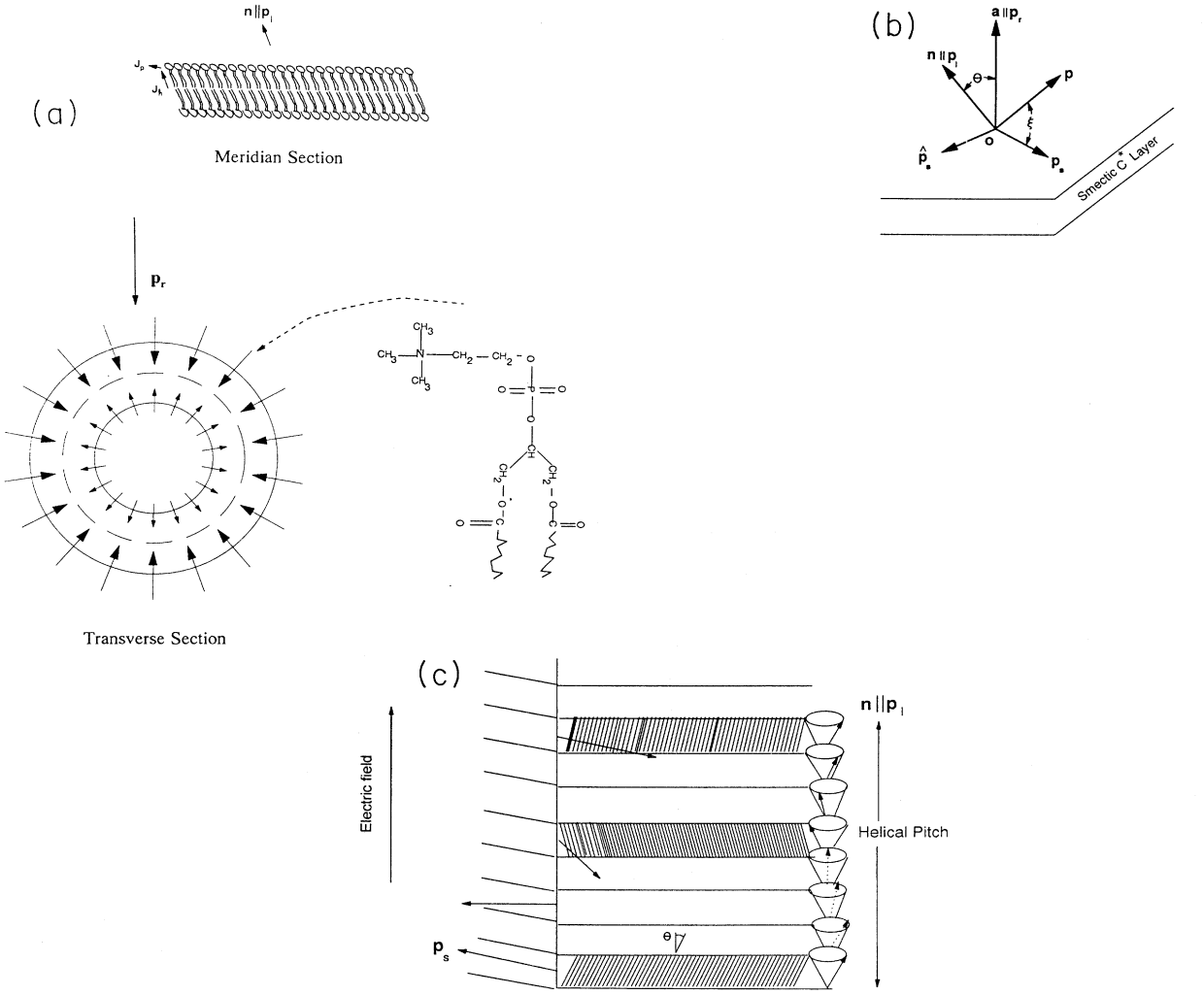

FIG. 4. (a) A fluid lipid bilayer is an example of 2D head-to-tail correlated Sm-C^* liquid crystal film, when the lipid molecules are tilted as shown in the meridian section of the cell membrane. The tilt originates from the fact that the zwitteronic head groups occupy more space laterally than the hydrocarbon chains [25]. When the bilayer is shaped into a cylindrical object, the outer monolayer has the lipids with the bulkier head groups. The transverse section shows the curvature-induced or flexoelectric origin of the net longitudinal electric polarization $\mathbf{p}_r$: the dipoles in the expanded outer monolayer increase, while those in the compressed inner monolayer decrease. As a result, the bilayer is polarized. The flexoelectric coefficient e is negative for this case. e can also be positive corresponding to the case in which the dipoles of the outer monolayer decrease, while those of the inner monolayer increase. Both have been observed [27]. The origin of the lipid dipole is in the chemical structure of the head group, shown on the bottom right. The head group conformational variations can cause lipid dipole moment changes, as noted above. The wiggly lines stand for fluid hydrocarbon chains. (b) Spontaneous electric polarization in a smectic-C^* layer. **a** is the layer normal vector and **n** is the molecular director. The steric dipole vector $\mathbf{p}_s$ is perpendicular to the **no**a plane. **p** is the electric dipole vector whose projection on the **no**a plane is $\mathbf{p}_l$, i.e., **p** is the vector sum of $\mathbf{p}_l$ and $\mathbf{p}_s$. The vector $\hat{\mathbf{p}}_s$ is perpendicular to $\mathbf{p}_s$ in the layer plane. (c) 3D head-to-tail correlated Sm-C^* liquid crystal may possess global longitudinal $\mathbf{p}_l$ and local transverse $\mathbf{p}_s$ ferroelectricity. The phase has a helicoidal twist, each layer having the same tilt angle θ. However, the **c** director rotates about the helix direction from layer to layer. The transverse electric polarization vector $\mathbf{p}_s$, which always remains perpendicular to the **c** director [cf. Figs. 1 and 4(a)] in the smectic layer plane, behave similarly. The longitudinal polarization $\mathbf{p}_l$ also rotates about the helix axis, always being inclined at an angle θ. Over macroscopic dimensions, the phase possesses no net transverse electric polarization, but may possess a net longitudinal electric polarization. An example may be myelin (see Sec. IX).

$$p_r = e\left[\frac{1}{R_1}+\frac{1}{R_2}\right],$$

where R_1 and R_2 are the two principal radii of curvature of the membrane. e is a flexoelectric coefficient, which can be positive or negative [see Fig. 4(a)]. Petrov and Pavloff [27] modeled the bilayer membrane by a bimorph composed of two halves of piezoelectric material with opposite directions of the polar axes and, assuming no trans-bi-layer exchange (which is normally a slow process), derived an expression for the flexoelectric coefficient e:

$$e = -\left[\frac{d\mu}{dA}\right]_{\bar{A}},$$

where μ is the normal component of the lipid dipole moment, A^o and A^i are the area per head group of the outer and inner monolayers respectively, and $\bar{A}$ is the area per head group of the midplane of the bilayer (nonstretched). From the measurements of surface potential difference across lipid monolayers spread on an air-water or a oil-water interface, Petrov and Pavloff [27] estimated e values for single-component lipids (lecithins).

Each monolayer half of the bilayer membrane is head-to-tail correlated, i.e., all the dipolar head groups are on one side and nonpolar hydrocarbon tails on the other. Head groups face the polar aqueous environment. Structural studies using deuterium NMR [28,29] indicate that the hydrocarbon chain segmental order parameter is constant across the bilayer. It is thus reasonable to use a single tilt angle for the bilayer and assume the dipoles on the opposing monolayer surfaces to be coupled. This implies the existence of a net longitudinal polarization $\mathbf{p}_r$ as above, as well as a net transverse polarization $\mathbf{p}_s$. The consequence of no transmembrane dipolar coupling is explained in Sec. IX. These features of the cell membrane, e.g., the tilt angle, and the net longitudinal and transverse polarizations have their counterpart in a 2D head-to-tail correlated (i.e., like polar ends of the molecules on the same side over a correlated region) Sm-C^* film, considered in detail in the present work. The characteristics of the corresponding 3D system are shown in Fig. 4(c).

The net transverse polarization $\mathbf{p}_s$, alluded to above, results from the net alignment of steric dipoles in the apposed monolayer halves. In a single-component lipid monolayer built of optically active molecules, steric dipole alignment would lead to the generation of a spontaneous electric polarization $\mathbf{p}_s$ in the layer plane, but in a direction perpendicular to $\hat{\mathbf{p}}_s$, given by

$$\mathbf{p}_s = \mu_p(\mathbf{n}\cdot\mathbf{i}_z)(\mathbf{i}_z\times\mathbf{n}),$$

where the phenomenological constant μ_p is expressed in terms of model parameters as [21]

$$\mu_p = \tfrac{1}{4}[(\tilde{\rho}^2/k_BT)(\mathbf{S}\cdot\mathbf{p})\Delta(D^6/L)\tilde{\sigma}(2\alpha_\perp+15\delta\alpha+\delta\alpha_\perp)].$$

Here $\delta\alpha=\alpha_{zz}-(\alpha_{xx}+\alpha_{yy})/2$ is the anisotropy of molecular polarizability, $\alpha_\perp=\alpha_{xx}+\alpha_{yy}$ is the transverse molecular polarizability, and $\delta\alpha_\perp=\alpha_{xx}-\alpha_{yy}$ is the anisotropy of the transverse polarizability. Note that the polarization $\mathbf{p}_s$ is in a direction perpendicular to the plane formed by the layer normal vector $\mathbf{i}_z$ and the director $\mathbf{n}$, and depends on the angle between the steric dipole vector $\mathbf{S}$ and the electric dipole of the same molecule. The molecular length and diameter are represented by L and D, respectively; Δ reflects the chirality of the individual molecule i and is given by $\Delta=(\mathbf{p}_i\cdot\mathbf{a}_i)(\mathbf{p}_i\times\mathbf{m}_i\cdot\mathbf{a}_i)$; $\mathbf{p}_i$ is the electric dipole vector of molecule i; $\mathbf{a}_i$ is the long axis of the whole molecule; $\mathbf{m}_i$ is a vector joining the steric dipole and the electric dipole; $\tilde{\sigma}$ is the fraction of nearest-neighbor molecules located in the same smectic plane; and $\tilde{\rho}$ is the number density of molecules. The magnitude of the electric dipole vector $\mathbf{p}$ is different in the apposed monolayer halves, causing the appearance of a net transverse polarization $\mathbf{p}_s$.

For a multicomponent mixture of chiral lipid molecules

$$\mu_p = \sum x_j x_k \mu_{jk},$$

where x_j is the mole fraction of the jth component and μ_{jk} is determined by the interaction between a molecule of component j and a molecule of component k [21].

Not all lipid molecules need be chiral. Also, there are other achiral molecules present in the cell membrane which are not lipids. For a mixture of a chiral component A with achiral molecules B, the constant μ_p is given by

$$\mu_p = \mu_{AA}x_A^2 + \mu_{AB}x_Ax_B.$$

Here $\mu_{BB}=0$.

We now gather together all the elastic and the polarization terms needed for the total free energy expression

$$F = 2\pi\int_{R-d/2}^{R+d/2}\int r\,dr\,dx\left[\frac{1}{2}K_{11}\left[\frac{d\theta}{dx}\right]^2+\frac{1}{2}K_{11}\theta^2\left[\frac{d\phi}{dx}\right]^2+\frac{1}{2}K_{11}\left[\frac{1}{r}-C_0\right]^2+\left[\frac{A}{2r^2}+\frac{2\sigma}{d}\right]\theta^2\right.$$

$$\left.+\left[\frac{B}{2r^2}-\frac{2\sigma}{3d}\right]\theta^4+\frac{p_l^2}{2\chi_l}-Ep_l-\mu_p\theta p_s+\frac{p_s^2}{2\chi_s}\right], \tag{12}$$

or

$$F=\int dx\left\{\pi RK_b\left[\frac{d\theta}{dx}\right]^2+\pi RK_b\theta^2\left[\frac{d\phi}{dx}\right]^2+\pi RK_bC_0^2+\pi K_{11}\ln\left[1+\frac{d}{R-d/2}\right]-2\pi K_bC_0\right.$$
$$+\left[\pi A\ln\left[1+\frac{d}{R-d/2}\right]+4\pi R\sigma\right]\theta^2+\left[\pi B\ln\left[1+\frac{d}{R-d/2}\right]-\frac{4}{3}\pi R\sigma\right]\theta^4$$
$$\left.+2\pi Rd\left[\frac{p_l^2}{2\chi_l}-Ep_l-\mu_p\theta p_s+\frac{p_s^2}{2\chi_s}\right]\right\}, \tag{13}$$

and

$$F=\int dx\left\{\pi RK_b\left[\frac{d\theta}{dx}\right]^2+\pi RK_bC_0^2+\frac{\pi K_b}{R}-2\pi K_bC_0\right.$$
$$+\left[4\pi R\sigma+\frac{\pi Ad}{R}\right]\theta^2-\left[\frac{4}{3}\pi R\sigma-\frac{\pi Bd}{R}\right]\theta^4$$
$$\left.+2\pi Rd\left[\frac{p_l^2}{2\chi_l}-Ep_l-\mu_p\theta p_s+\frac{p_s^2}{2\chi_s}\right]\right\}, \tag{14}$$

where we have assumed, following Carlsson, Stewart, and Leslie [23], that $\phi=\phi(r,\alpha)$, μ_p is the piezoelectric coefficient [21], χ_s is the transverse dielectric susceptibility, χ_l is the longitudinal dielectric susceptibility, and C_0 is the spontaneous splay curvature which takes account of the chemically distinct monolayer halves. As no boundary condition is applied in the α direction, we further assume that $\phi(r,\alpha)=\phi(r)$. Since the membrane has very small radial extension, heterogeneity in ϕ along the r direction is negligible. Further, $\ln(1+x)\approx x$ for $x\ll 1$, which also has been used in Eq. (13), since $d/R\ll 1$.

Now, referring to Fig. 4(b), we find

$$p_l=p\sin\xi,\quad p_s=p\cos\xi\ . \tag{15}$$

The angle ξ [see Fig. 4(b)] is considered to be a material constant and can be experimentally determined from measurements of both p_l [27] and p_s [15]. Minimizing the free energy with respect to p, i.e., $\partial F/\partial p=0$,

$$p=(E\sin\xi+\theta\mu_p\cos\xi)\Xi(\xi)\ , \tag{16}$$

where

$$\Xi(\xi)\equiv\left[\frac{\sin^2\xi}{\chi_l}+\frac{\cos^2\xi}{\chi_s}\right]^{-1}.$$

Inserting the value of p from Eq. (16) into the energy expression gives

$$F=\int dx\left\{\pi RK_b\left[\frac{d\theta}{dx}\right]^2+\pi RK_b\left[\frac{1}{R}-C_0\right]^2+\left[\left[\frac{\pi Ad}{R}+4\sigma\pi R\right]-\pi Rd\Xi(\xi)\mu_p^2\cos^2\xi\right]\theta^2\right.$$
$$\left.+\left[\frac{\pi Bd}{R}-\frac{4\sigma\pi R}{3}\right]\theta^4-2\pi Rd\Xi(\xi)\mu_pE\theta\sin\xi\cos\xi-\pi RdE^2\sin^2(\xi)\Xi(\xi)\right\}. \tag{17}$$

Looking carefully at Eq. (17), we find a term proportional to $E\theta$, which means that there is a direct coupling of the electric field to the mechanical deformation θ. Propagation of electric fields and electrically induced mechanical fields in ferroelectric liquid crystals depends crucially on the presence of such coupling. If the molecules are achiral, i.e., the piezoelectric coefficient is zero, this term is absent and there cannot be an electrical solitary wave propagation or electrically induced mechanical field propagation, unless there is a dielectric mechanism connecting the electric and the mechanical fields [9]. Electrically induced propagation of a mechanical field, e.g., the tilt angle θ, is discussed in Sec. IV. For the propagation of an electrical wave form, there has to be a mechanism for the spatiotemporal variation of the transmembrane electric field, which is coupled to the spatiotemporal variation of the mechanical field θ. Such a mechanism is considered in Sec. V A.

A. The Landau–de Gennes approach

Equation (13) is analogous to the phenomenological Landau–de Gennes–type free energy used for ferroelectric smectic systems. For Sm-C^* liquid crystals, the free-energy density is [30,31]

$$F'=\check{a}(\xi_1^2+\xi_2^2)+\check{b}(\xi_1^2+\xi_2^2)^2+\frac{1}{2}K\left[\left[\frac{\partial\xi_1}{\partial z}\right]^2+\left[\frac{\partial\xi_2}{\partial z}\right]^2\right]+\lambda\left[\xi_1\frac{\partial\xi_2}{\partial z}-\xi_2\frac{\partial\xi_1}{\partial z}\right]$$
$$-\mu_p(p_x\xi_2-p_y\xi_1)-\mu_f\left[p_x\frac{\partial\xi_1}{\partial z}+p_y\frac{\partial\xi_2}{\partial z}\right]-pE+\frac{p^2}{2\chi}\ , \tag{18}$$

where the layer normal is assumed to be in the z direction and the electric field is assumed in the x direction. The fourth term is the Lifshitz invariant, p is the magnitude of the electric polarization vector, $\check{a}$ and $\check{b}$ are the phenomenological coefficients, and μ_p and μ_f are the piezoelectric and flexoelectric coefficients, respectively. The two-component tilt vector order parameter is expressed in terms of $\mathbf{n}$ or θ, and the azimuthal angle ϕ as in Eq. (7). Out of the four terms in Eq. (6), the one that appears in Eq. (18) is significant relative to the others near the Sm-C^*–Sm-A transition.

For the head-to-tail correlated Sm-C^* liquid crystal, we need to add contributions from the longitudinal electric polarization p_l. Also, the electric field is in the z direction. Because of the thinness of the membrane, the z dependence of the order parameters is ignored. Borrowing relevant terms from Eq. (6), we write the free-energy density as

$$F'=\check{a}(\xi_1^2+\xi_2^2)+\check{b}(\xi_1^2+\xi_2^2)^2 + \frac{1}{2}K'\left[\frac{\partial\xi_1}{\partial x}+\frac{\partial\xi_2}{\partial y}\right]^2+\frac{1}{2}K''\left[\frac{\partial\xi_1}{\partial y}-\frac{\partial\xi_2}{\partial x}\right]^2 + \mu_p(p_x\xi_2-p_y\xi_1)+\frac{p_s^2}{2\chi_s}+\frac{p_l^2}{2\chi_l}-Ep_l \ .$$

Noting that

$$p_x=-p_s\sin\phi, \quad p_y=p_s\cos\phi \ ,$$

with p_l and p_s given by Eq. (15), and in view of the one-constant approximation $K\equiv K'=K''$, we derive

$$F'=\check{a}\theta^2+\check{b}\theta^4+\tfrac{1}{2}K[(\nabla\theta)^2+\theta^2(\nabla\phi)^2] -\mu_p p_s\theta+\frac{p_s^2}{2\chi_s}+\frac{p_l^2}{2\chi_l}-Ep_l \ .$$

This agrees very well with Eq. (13).

In invoking the phenomenological Landau–de Gennes approach here, we have tried to find a rationale for use of the B coefficients in Eq. (9). In the original format of Carlsson, Stewart, and Leslie [22], the B coefficients were missing and, as a result, a fourth-power term in θ in the free-energy expression did not appear.

B. Longitudinal ferroelectricity in polar smectic-A systems

The Landau–de Gennes approach has also been applied to polar systems which exhibit rich smectic-A polymorphism [32]. In nonpolar smectic-A and polar single-layer smectic-A_1 systems, only the mass density wave $\rho(z)=\rho_0\cos(k_1 z)$ exists. However, in general cases of polar systems with high electric dipole moments, a collinear electric polarization wave $\Phi(z)=\Phi_0\cos(k_2 z)$ can coexist with the mass density modulation. Obviously, the periods of the modulations ($2\pi/k_1$ for the density and $2\pi/k_2$ for the polarization) are not commensurate. The period $2\pi/k_1$ is comparable with the molecular length l_1, while the period $2\pi/k_2$ is determined by the dimension l_2 of the antiparallel cluster of two molecules, with $l_1<l_2<2l_1$. Switching on the interaction (i.e., coupling terms in the free-energy expression) gives a variety of commensurate and incommensurate structures (solitons) as a result of phase transitions.

Essentially the same kind of free-energy expression as Eq. (13) is expected, except that the tilt angle θ for the Sm-C^* system needs to be replaced by the mass density as the order parameter. Prost and Barois [32] have considered a generalized free energy with a variety of complicated coupling schemes. We write the free-energy density with a bilinear coupling term as

$$F_{p\rho}=a_1\rho^2+b_1\rho^4+\left[\frac{\partial\rho}{\partial x}\right]^2+\frac{p^2}{2\chi}+C'p\rho-Ep \ ,$$

where χ is the dielectric susceptibility. Obviously, results similar to those in Eq. (13) are obtained in this case also.

Prost and Barois [32] predicted that these polar smectic-A systems could be longitudinal ferroelectric if the ratio of the distance between the two neighboring solitons over the bilayer spacing is a half-integer.

IV. SOLITON EQUATION

Liquid crystals are viscoelastic, so that the dynamical deformations are damped and subject to increasing elastic forces. The time dependence of the tilt angle θ is then determined by a simple balance between a friction term $\gamma\partial\theta/\partial t$ and the energy gain that provides the driving force.

Thus, minimizing F, given by Eq. (17), with respect to θ and equating the result to a viscous damping term $\gamma\partial\theta/\partial t$ leads to the Euler-Lagrange equation

$$\gamma\frac{\partial\theta}{\partial t}=\pi RK_b\frac{\partial^2\theta}{\partial x^2}-(a\theta^3-b\theta-\bar{c}E) \ , \tag{19}$$

where

$$a\equiv 4\pi R\left[\frac{Bd}{R^2}-\frac{4\sigma}{3}\right] \ ,$$

$$b\equiv 2\pi R\left[-\left[\frac{Ad}{R^2}+4\sigma\right]+d\Xi(\xi)\mu_p^2\cos^2\xi\right] \ ,$$

and

$$\bar{c}\equiv\pi Rd\mu_p\Xi(\xi)\sin\xi\cos\xi \ .$$

Using dimensionless independent variables, we write Eq. (19) in the form

$$\frac{\partial\theta}{\partial T}=\frac{\partial^2\theta}{\partial X^2}+F_E(\theta) \ , \tag{20}$$

where

$$T\equiv\frac{t}{t_0}, \quad t_0\equiv\frac{\gamma}{a} \ ,$$

$$X\equiv\frac{x}{x_0}, \quad x_0\equiv\left[\frac{\pi RK_b}{a}\right]^{1/2} \ ,$$

and

$$F_E(\theta)\equiv-\theta^3+\frac{b}{a}\theta+\frac{\bar{c}E}{a}\equiv-\frac{\partial V_E(\theta)}{\partial\theta} \ . \tag{21}$$

The discriminant of the equation $F_E(\theta)=0$ is

$$\Delta\equiv\left[\frac{q'}{2}\right]^2+\left[\frac{p'}{3}\right]^3=\left[-\frac{\tilde{c}E}{2a}\right]^2+\left[-\frac{b}{3a}\right]^3\le 0\ .$$

Therefore,

$$c\equiv\tilde{c}E\le\frac{2b^{3/2}}{3\sqrt{3a}}\equiv c_0\ . \tag{22}$$

The real roots are

$$\theta_1=\sqrt{b/a}\ \cos(\theta_0+2\pi/3)\ ,$$
$$\theta_2=\sqrt{b/a}\ \cos(\theta_0+4\pi/3)\ ,$$
$$\theta_3=\sqrt{b/a}\ \cos\theta_0\ ,$$

where

$$\theta_0\equiv\tfrac{1}{3}\cos^{-1}\left[\frac{c}{c_0}\right],\quad \theta_1\le\theta_2<\theta_3\ .$$

The potential function $V_E(\theta)$ is given as

$$V_E(\theta)=\frac{1}{4}\theta^4-\frac{b}{2a}\theta^2-\frac{\tilde{c}E}{a}\theta\ . \tag{23}$$

To conform to the nomenclature used in later sections [e.g., Eq. (26) in Sec. V], we define $u\equiv(3a/b)^{1/2}\theta$ and $w\equiv(3a/b^3)^{1/2}\tilde{c}E$, where w is a constant ($w=-0.5344$ for the present case. Then

$$V_w(u)=\frac{1}{3}\left[\frac{b}{a}\right]^2\left[\frac{1}{12}u^4-\frac{1}{2}u^2-wu\right]\ .$$

Figure 5(a) shows $V_w(u)$ versus u variation. However, for the rest of the present section, we continue to work

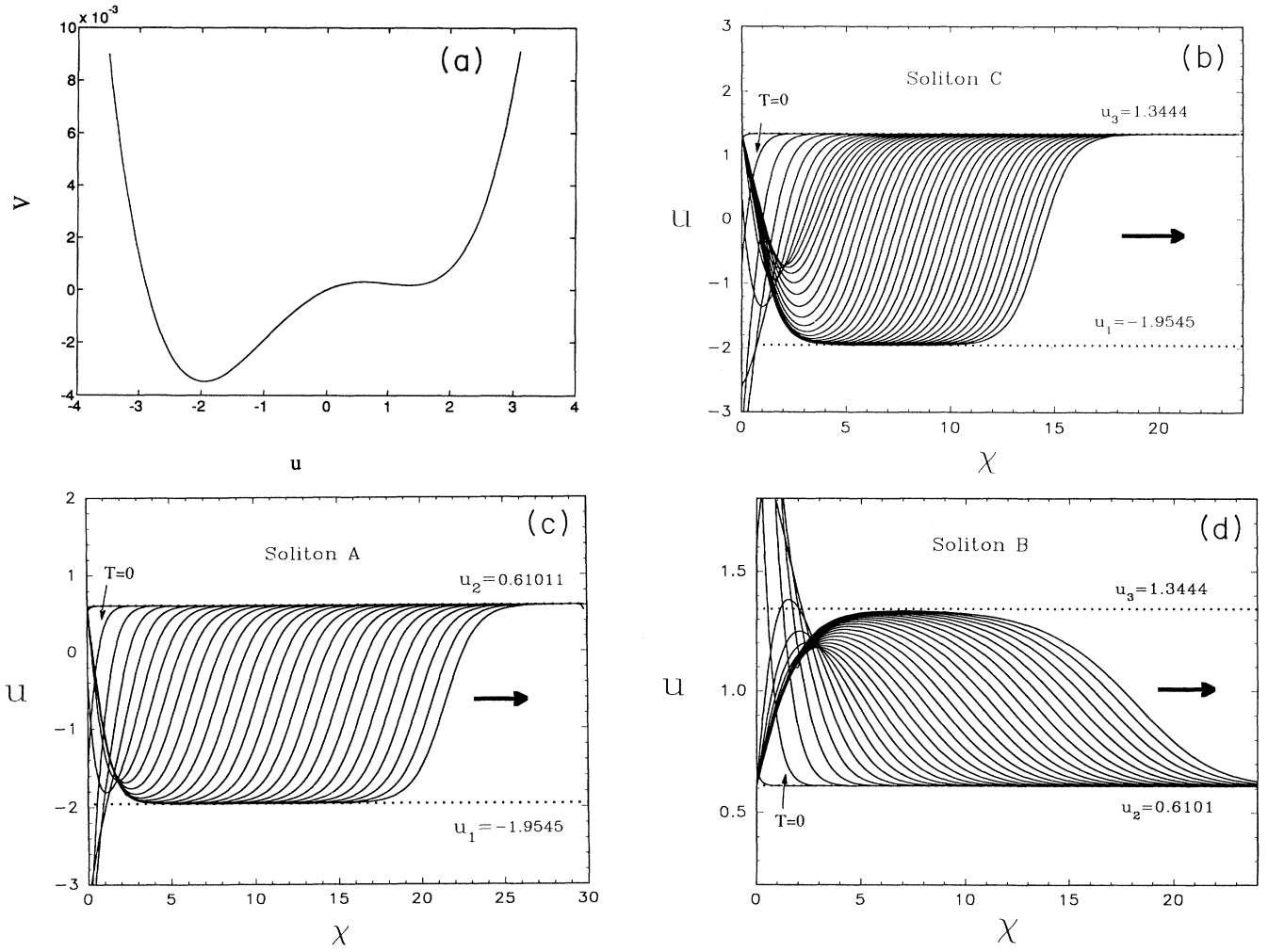

FIG. 5. (a) Graph of the potential function given by Eq. (23) with $a=1.291$, $b=0.1$, and $w=-0.534\,406$. (b)–(d) A boundary value problem for Eq. (20) with $a=1.291$, $b=0.1$, and $w=-0.534\,406$. The resting solutions are $u_1\equiv(3a/b)^{1/2}\theta_1=-1.9545$, $u_2\equiv(3a/b)^{1/2}\theta_2=0.610\,106$, and $u_3\equiv(3a/b)^{1/2}\theta_3=1.344\,441$. $\chi\equiv(b/a)^{1/2}X$. On the line $T=0$, $u=u_0$, where $\partial u/\partial T=0$. On the line $\chi=0$, $u=F(T)=u_0+H[1-\cos(2\pi T/T_0)]$ for $0<T\le T_0$ and $u=u_0$ for $T\ge T_0$. (b) Soliton C, $u_0=1.3444$ and $H<0$; (c) soliton A, $u_0=0.610\,106$ and $H<0$; (d) soliton B, $u_0=0.610\,106$ and $H>0$. The time increment between successive curves is 0.5 for all three cases.

with θ and E. Using Eq. (21) in Eq. (20) results in the standard θ^4-soliton equation [33]. In the absence of an electric field ($E=0$), we obtain

$$V_0(\theta)=-\frac{b}{2a}\theta^2+\frac{1}{4}\theta^4 .$$

The extrema occur at $\theta=\pm(b/a)^{1/2}$ and $V_0(\theta)$ is a symmetric "double-well" potential. We will show that a particular soliton solution is precluded for this case.

When the electric field is applied such that its magnitude is lower than a cutoff value E_0, an asymmetric profile is obtained [see Fig. 5(a)]. For Eq. (20) to have a soliton solution, the potential $V_E(\theta)$ [Eq. (23)] must have two minima and one maximum (or one minimum and an inflection point), i.e.,

$$\left[\frac{\partial V_E}{\partial\theta}\right]_{E=E_0}=0=\left[\frac{\partial^2 V_E}{\partial\theta^2}\right]_{E=E_0} .$$

Now

$$\theta_i^3-\frac{b}{a}\theta_i-\frac{c_0}{a}=0$$

and

$$3\theta_i^2-b/a=0 ,$$

that is,

$$c_0=\frac{2}{3\sqrt{3}}\frac{b^{3/2}}{a^{1/2}} , \tag{24}$$

which agrees perfectly with Eq. (22).

The range of stability of the soliton can be obtained from Eqs. (22) and (24). In the following, we present the possible soliton solutions to Eq. (20). There are three kinds of solitons [33]. Fronts propagating from "stable" state θ_1 to stable state θ_3 are indicated in Fig. 5(b) as soliton C and correspond to a ball rolling from the right-hand minimum to the left-hand minimum in Fig. 5(a). Fronts propagating from stable state θ_1 to "unstable" state θ_2 are represented by soliton A and correspond to a ball rolling from the maximum to the left-hand minimum [see Figs. 5(a) and 5(c)]. Soliton B stands for fronts propagating from stable state θ_3 to unstable state θ_2 and corresponds to a ball rolling from the maximum to the right-hand minimum in Fig. 5(a). It has a shape opposite that of solitons A and C [see Figs. 5(a) and 5(d)].

There are three possible solitons: A, B, and C. Only soliton C requires an electric field and the form of the solution is given as

$$\theta_C=\left[\frac{b}{a}\right]^{1/2}[\cos\theta_0-\cos(\theta_0+2\pi/3)]\{1-\tanh[W_C^{-1}(X-X_0-C_CT)]\}+\left[\frac{b}{a}\right]^{1/2}\cos(\theta_0+2\pi/3)$$
$$=\left[\frac{3b}{a}\right]^{1/2}\sin(\theta_0+\pi/3)\{1-\tanh[W_C^{-1}(X-X_0-C_CT)]\}+\left[\frac{b}{a}\right]^{1/2}\cos(\theta_0+2\pi/3) ,$$

where

$$W_C=\sqrt{2}\left\{\left[\frac{b}{a}\right]^{1/2}[\cos\theta_0-\cos(\theta_0+2\pi/3)]\right\}^{-1}$$
$$=\left[\frac{2}{3}\right]^{1/2}\left[\left[\frac{b}{a}\right]^{1/2}\sin(\theta_0+\pi/3)\right]^{-1} .$$

In dimensional units,

$$w_C=\left[\frac{2\pi RK_b}{3a}\right]^{1/2}\left[\left[\frac{b}{a}\right]^{1/2}\sin(\theta_0+\pi/3)\right]^{-1}$$
$$=\left[\frac{2\pi RK_b}{3b}\right]^{1/2}\csc(\theta_0+\pi/3) .$$

Also,

$$C_C=\left[\frac{b}{2a}\right]^{1/2}[\cos\theta_0+\cos(\theta_0+2\pi/3)-2\cos(\theta_0+4\pi/3)]$$
$$=3\left[\frac{b}{2a}\right]^{1/2}\cos(\theta_0+\pi/3)$$

and in dimensional units

$$c_C=\frac{3}{\gamma}\left[\frac{\pi RK_b b}{2}\right]^{1/2}\cos(\theta_0+\pi/3) .$$

The velocities and half-widths of solitons A and B are recorded in Appendix A. Note that as the electric field $E\to 0$, the wave speed $c_C\to 0$, but not c_A or c_B. This means that solitons A and B can propagate without the electric field. However, as previously mentioned, the propagating soliton C requires an electric field. Some of the properties of this soliton are listed as [8] follows.

(i) There exists a unique solitary wave solution such that

$$\theta\equiv\theta^*(x-c^*t)\equiv\theta^*(\xi) ,$$
$$\lim_{\xi\to-\infty}\theta^*(\xi)=\theta_1,\quad \lim_{\xi\to\infty}\theta^*(\xi)=\theta_3 ,$$
$$\theta^{*\prime}(\xi)<0 .$$

(ii) There exists bistable behavior, i.e., θ_1 and θ_3 are stable and θ_2 unstable.

(iii) c^*, the critical speed (the speed of the asymptotic

wave form), is completely determined by the function $F(\theta)$.

The relation

$$c^* \lesseqgtr 0 \leftrightarrow \int_{\theta_3}^{\theta_1} F_E(\theta)\, d\theta \lesseqgtr 0$$

is valid. This is easy to see because

$$\int_{\theta_3}^{\theta_1} F_E(\theta)\, d\theta = V_E(\theta_1) - V_E(\theta_3) \ .$$

This integral is zero when $E=0$ and the behavior of the wall is static. (See Sec. VIII.)

For $c/c_0 \ll 1$, to first order in c/c_0, we obtain

$$c_C \approx \frac{3\sqrt{3}}{2\sqrt{2}} \frac{c\sqrt{a}}{\gamma b} (\pi R K_b)^{1/2} \ . \tag{25}$$

This is possible since for $c=0$, $\theta_0=\pi/6$ and $\cos(\pi/3+\theta_0)=0$. It is again clear from Eqs. (25), (A1), and (A2) that solitons A and B can propagate without the electric field, whereas soliton C cannot. At present we are unable to calculate the speed of the soliton using Eq. (25) and compare the result to observed values because some of the physical quantities representing the membrane have not yet been determined.

The solitary wave nature of the solutions is not destroyed even when the rotational kinetic energy, $\frac{1}{2}I(\partial\theta/\partial t)^2$ is accounted for in Appendix B [34]. The results for this case are given there.

V. HODGKIN-HUXLEY EQUATIONS

The traveling electrically induced soliton is just a special case of the Fitzhugh-Nagumo model, which consists of the coupled set of equations [6,7]

$$\begin{aligned} h_0 \frac{\partial^2 u}{\partial x^2} &= \frac{1}{c_0}\frac{\partial u}{\partial \tau} + \left[\frac{u^3}{3} - u - w\right] \ , \\ c_0 \frac{\partial w}{\partial \tau} + b_0 w &= a_0 - u \ , \end{aligned} \tag{26}$$

where a_0, b_0, and c_0 are constants satisfying the relations $0<b_0<1$, $(c_0)^2>b_0$, and $1-b_0/2<a_0<2$. The variables u, w, and $h_0\partial^2 u/\partial x^2$ in Eq. (26) correspond to the pair of variables (V_m, m), the pair of variables (h,n), and I_m in Eq. (27), and x is the distance in the direction of the axon. Here the variables and coefficients correspond to those used by Nagumo, Arimoto, and Yoshizawa [7]. We will obtain a similar equation; however, the variables and coefficients will correspond to our soliton model.

The basic physical system being considered here is the Bonhoeffer–van der Pol (BVP) model [6,7]. For the "space clamp," that is, in the case where the excitation of the nerve axon is spatially uniform (synchronous action of the "patches" in the membrane), the left-hand side of the first of the two equations of Eq. (26) is replaced by zero or a constant [35]. Figure 6(a) shows the trajectories in the (u,w) plane of the BVP model in the space-clamp situation where the left-hand side of the first equation of the coupled set is zero.

This coupled set of partial differential equations have been shown to have the same kind of propagating soliton solution as the Hodgkin-Huxley (HH) set of partial differential equations [1]. The complete set of equations is reproduced in Appendix C. Here we give the equation partitioning the total transmembrane current into a capacity current and ionic currents due to the movement of sodium, potassium, and other ions [1]:

$$\begin{aligned} I_m = C_m \frac{dV_m}{dt} &+ \bar{g}_{\mathrm{Na}} m^3 h (V_m - E_{\mathrm{Na}}) \\ &+ \bar{g}_{\mathrm{K}} n^4 (V_m - E_{\mathrm{K}}) + \bar{g}_L (V_m - E_L) \ . \end{aligned} \tag{27}$$

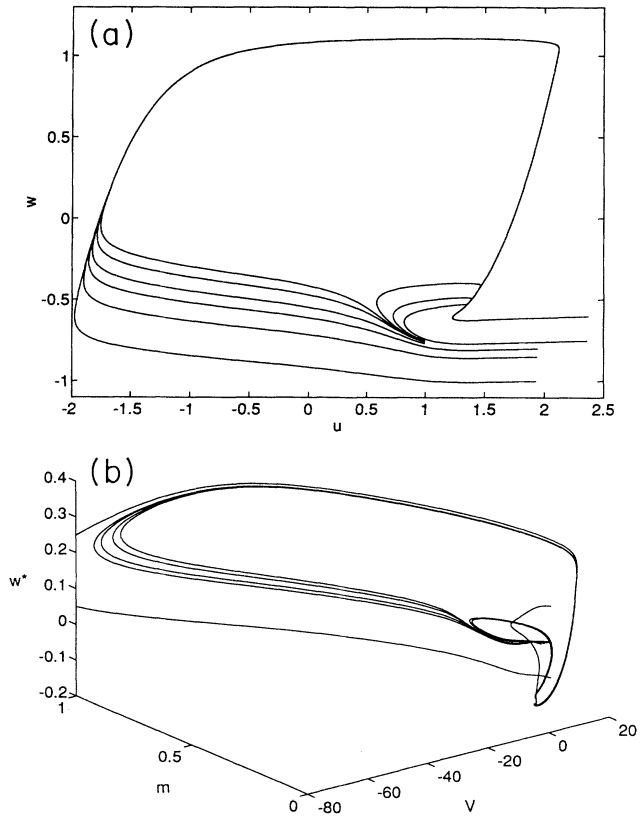

FIG. 6. (a) Phase plane and physiological state diagram of the BVP model [Eq. (26)]: $a_0=1.291$, $b_0=0.1$, and $c_0=4.5$; $u_0=1.344\,44$ and $w_0=-0.534\,406$ are the coordinates of the resting point. A threshold phenomenon (TP) separatrix runs along the black solid line dividing the phase plane into an active regenerative region (to the left of the separatrix) from a refractory region (to the right of the separatrix). Excitation (i.e., action potential) occurs whenever the phase point is displaced across the separatrix from left to right. When the displacement is not enough to take the phase point across the separatrix, the action potential cannot result and such subthreshold stimuli decay fast. (b) Hodgkin-Huxley (HH) physiological state diagram. The BVP physiological state diagram has its counterpart in the HH model, obtainable by projection from the four-dimensional (V,m,n,h) phase space. The resting point is given by $(V_0, m_0, w_0^*)=(0, 0.052\,93, -0.1342)$. The TP separatrix is easily identifiable.

The symbols are described in Appendix C; V_m is the membrane potential and E_α corresponds to the Nernst potential of the α ionic species. Fitzhugh [6] argued that the pair of variables (V,m) correspond to u^*, which reflects membrane excitability and changes relatively rapidly. Variables (h,n) correspond to w^*, which represents accommodation and refractoriness and changes relatively slowly. During the time course of the action potential, the curves n and $-h$ behave similarly [35]. Thus n and $-h$ can be replaced by their average $w^*=\frac{1}{2}(n-h)$. Points from the (n,h) plane can be projected perpendicularly on to the w^* axis, by projection along lines of constant w^*. Similarly, points of the (V,m) plane can be projected along lines of constant u^*, where $u^*=V-36m$, according to Fitzhugh [6]. If one plots the trajectories in the (u^*,w^*) plane for the case $I_m=0$, fair agreement between the BVP and the HH models is apparent [6]. In Fig. 6(b) we show the 3D (V,m,w^*) diagram. It is not a phase-plane diagram, but a useful expository device for comparing the HH and BVP models. The qualitative similarity between Figs. 6(a) and 6(b) implies that two-dimensional models such as the BVP equations can reproduce the same kind of excitable-oscillatory behavior as the four-dimensional HH equations.

For uniform propagation, the space-time behavior of $V_m(x,t)$ must satisfy the traveling wave form, i.e.,

$$V_m(x,t)=V_m(x-c_s t)\ ,$$

where c_s is the velocity of propagation. Using the chain rule twice gives

$$\frac{\partial^2 V_m}{\partial x^2}=\frac{1}{c_s^2}\frac{\partial^2 V_m}{\partial t^2}\ .$$

For a cylindrical geometry

$$I_m=\frac{R}{2\tilde{R}_i}\frac{\partial^2 V_m}{\partial x^2}\ ,$$

where R is the radius of the axon and $\tilde{R}_i$ is the specific resistance of the axoplasm. Combining these equations, we obtain

$$\frac{R}{2\tilde{R}_i c_s^2}\frac{\partial^2 V_m}{\partial t^2}=C_m\frac{\partial V_m}{\partial t}+g_{\mathrm{K}}(V_m-E_{\mathrm{K}})+g_{\mathrm{Na}}(V_m-E_{\mathrm{Na}})+g_L(V_m-E_L)\ . \quad (28)$$

Hodgkin and Huxley solved this nonlinear equation numerically [1]. Other computer techniques are now available [35]. In Appendix C we describe a numerical technique for solving this five-dimensional equation.

However, without solving Eq. (28) explicitly, one important result can be obtained, namely, any solution $V_m(x,t)$ will continue to be a solution if

$$\frac{R}{2\tilde{R}_i c_s^2}=\text{const}\equiv\frac{1}{K_0},\quad c_s=\left[\frac{RK_0}{2\tilde{R}_i}\right]^{1/2}\ .$$

Since K_0 is an unknown constant, one pair of experimental values of c_s and R is required. Thereafter, c_s can be predicted for any other radius R and $c_s\propto R^{1/2}$. Experimentally, these predictions are well confirmed [35].

A. Nernst-Planck equation

The excitable nerve membrane ($\sim$75 Å thick) has a resting membrane potential difference $V_{\mathrm{in}}-V_{\mathrm{ex}}\approx-0.1$ V, which implies a strong transmembrane electric field of about 10^5 V/cm. Ions such as sodium (Na^+), potassium (K^+), and chloride (Cl^-) exist on both the intracellular and the extracellular sides, being subject to diffusional and electric field forces. We write the membrane capacity current as the balance between the diffusion currents, ion pump currents, and the current due to the electric field (the Nernst-Planck equation) [35,36]:

$$Cd\frac{dE}{dt}=-F\sum_j D_j\frac{d[j]}{dx}-\frac{F^2E}{R'T}\sum_j D_j[j]+\sum_j I_j^p\ ,$$

where C is the membrane capacitance and $j=\mathrm{Na}^+,\mathrm{K}^+,\mathrm{Cl}^-$. The first term on the right-hand side gives the diffusion electric current driven by the transmembrane concentration gradient of the jth species, the second term represents the current due to the electric field given by the transmembrane potential gradient, and I_j^p is the current due to the active j ion pumps. Under the resting condition, the ion fluxes due to the first two terms are opposite each other. D_j is the diffusion coefficient of the jth ionic species. F, R', and T are the Faraday constant, the gas constant, and the absolute temperature, respectively. Now, in the second term of the equation, we replace $[j]$ by $[j]_{\mathrm{av}}$, the average concentration of jth ionic species in the membrane, given by

$$[j]_{\mathrm{av}}=\beta_j\left[\frac{C_iV_i+C_eV_e}{V_i+V_e}\right]\ ,$$

where V_i and V_e are the intracellular and extracellular volumes and β_j is the partition coefficient which relates the concentration of an ion species in the bulk to that in

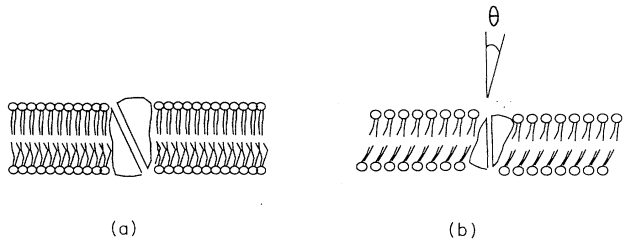

FIG. 7. Schematic of how an ion channel in a nerve membrane can be affected by the direction of lipid molecules. The direction of the molecules can determine the geometrical configuration of the channel and/or change the position of the charged groups that affect the potential seen by a positive ion, thereby affecting the mobility of a channel (or, in other words, the permeability of the ion). (a) When the lipid molecules are untilted, the ion channel allows no or partial ion transmission. (b) When the lipid molecules are tilted by an appropriate amount ($\theta=\theta_j^0$), the ion channel is open.

the membrane by $[j]_i=\beta_j C_i$ and $[j]_e=\beta_j C_e$. The $[j]$'s are concentrations in the membrane and the C's are bulk concentrations. The subscripts i and e stand for intracellular and extracellular, respectively. The average ionic concentrations are constants while the intracellular and extracellular ionic concentrations $[j]_i$ and $[j]_e$ are variable. Under the resting condition ($E=E_0$),

$$I_j^p=\frac{FD_j}{d}\Delta[j]_{\text{rest}}+\frac{F^2E_0}{R'T}D_j[j]_{\text{av}} ;$$

hence $\Delta[j]_{\text{rest}}$, the concentration difference of the j ionic species on the two sides of the membrane, can be found. The quantity d, as in Sec. II, is the membrane thickness.

In our Sm-C^* model of the cell membrane, the concentration gradient of each ionic species across the membrane is assumed to be tilt-angle dependent. This is consistent with Fig. 7 and the speculation of Hodgkin and Huxley, which is stated in the opening sentence of the present work. The ion channel for species j is completely open at $\theta=\theta_j^0$ ($j=\text{Na}^+,\text{K}^+,\text{Cl}^-$) wiping out the concentration gradient of the species between the intracellular and the extracellular regions. Thus

$$[j]_e-[j]_i=f(\theta)=f(\theta_j^0)+(\theta-\theta_j^0)f'(\theta_j^0)+\cdots$$

$$=(\theta-\theta_j^0)f'(\theta_j^0) ,$$

neglecting higher-order terms in the Taylor expansion of $f(\theta)$. $f'(\theta_j^0)$ is determined from the fact that the concentration difference on the left-hand side corresponds to that for the resting condition for $\theta=\theta_j^p$, yielding

$$f'(\theta_j^0)=\frac{\Delta[j]_{\text{rest}}}{(\theta_j^p-\theta_j^0)} .$$

$\Delta[j]_{\text{rest}}$ is determined by the transport rate and density of ion pumps. Thus we write

$$Cd\frac{dE}{dt}=-\frac{F}{d}\sum_j D_jf'(\theta_j^0)(\theta-\theta_j^0)-\frac{F^2E}{R'T}\sum_j D_j[j]_{\text{av}}$$
$$+\frac{F}{d}\sum_j D_j\Delta[j]_{\text{rest}}+\frac{F^2E_0}{R'T}\sum_j D_j[j]_{\text{av}}$$

or

$$\frac{dE}{dt}+\frac{F^2E}{R'TdC}\sum_j D_j[j]_{\text{av}}$$
$$=\frac{F}{d^2C}\sum_j D_jf'(\theta_j^0)\theta_j^0-\frac{F\theta}{d^2C}\sum_j D_jf'(\theta_j^0)$$
$$+\frac{F}{Cd^2}\sum_j D_j\Delta[j]_{\text{rest}}+\frac{F^2E_0}{R'TCd}\sum_j D_j[j]_{\text{av}} . \quad (29)$$

The movement of θ towards θ_j^0 implies passive transmembrane transport of the ion species j. Active transmembrane transport is initiated by ion pumps, which operate to restore the electrochemical gradient of ion species j, and means the movement of θ away from θ_j^0 (i.e., in the reverse direction).

B. The soliton model for the Fitzhugh-Nagumo equations

Equations (19) and (29) have exactly the same form as the Fitzhugh-Nagumo equations (26) under the following changes of variables:

$$\tau\equiv\frac{t}{(\gamma/\beta\tilde{c})^{1/2}},\quad u\equiv\left[\frac{3a}{b}\right]^{1/2}\theta ,$$
$$b_0\equiv\frac{bF^2}{\beta\tilde{c}R'TdC}\sum_j D_j[j]_{\text{av}} ,$$
$$w\equiv\frac{\sqrt{3}\tilde{c}a^{1/2}}{b^{3/2}}E,\quad h_0\equiv\frac{\pi RK_b}{b},\quad c_0=\frac{b}{\sqrt{\tilde{c}\gamma\beta}} ,$$
$$a_0\equiv\left[\frac{3a}{b\beta^2}\right]^{1/2}\left[\frac{F}{Cd^2}\sum_j f'(\theta_j^0)\theta_j^0D_j\right.$$
$$+\frac{F}{Cd^2}\sum_j D_j\Delta[j]_{\text{rest}}$$
$$\left.+\frac{F^2E_0}{R'TCd}\sum D_j[j]_{\text{av}}\right] ,$$

where

$$\beta\equiv\frac{F}{Cd^2}\sum_j D_jf'(\theta_j^0) .$$

Combining the two equations of the FN set, thus eliminating E, we obtain

$$c_0h_0\frac{\partial^3u}{\partial\tau\partial x^2}+b_0h_0\frac{\partial^2u}{\partial x^2}$$
$$=\frac{\partial^2u}{\partial\tau^2}-c_0\left[\left[1-\frac{b_0}{c_0^2}\right]-u^2\right]\frac{\partial u}{\partial\tau}$$
$$+(1-b_0)u+\frac{b_0}{3}u^3-a_0 . \quad (30)$$

The behavior of an imparted impulse as it approaches the asymptotic soliton shape is described by a boundary-value problem using Eq. (30) and is shown in Fig. 8.

Using the dimensionless scaled variables

$$x'\equiv\frac{x}{\sqrt{c_0h_0}},\quad z\equiv 2a_0\frac{(a_0-u)}{a_0^2-1} ,$$
$$\mu\equiv c_0(a_0^2-1),\quad \varepsilon\equiv\frac{a_0^2-1}{4a_0^2},\quad \Omega\equiv b_0(a_0^2-1) , \quad (31)$$

we obtain

$$\frac{\partial^3z}{\partial\tau\partial x'^2}+\frac{b_0}{c_0}\frac{\partial^2z}{\partial x'^2}$$
$$=\frac{\partial^2z}{\partial\tau^2}+\left[\mu(1-z+\varepsilon z^2)+\frac{b_0}{c_0}\right]\frac{\partial z}{\partial\tau}+(1+\Omega)z$$
$$-\frac{1}{2}\Omega z^2+\frac{1}{3}\varepsilon\Omega z^3+(\Omega+b_0)\left[-2+\frac{1}{3\varepsilon}\right] .$$

For simplicity, Nagumo, Arimoto, and Yoshizawa [7] set $b_0=0$.

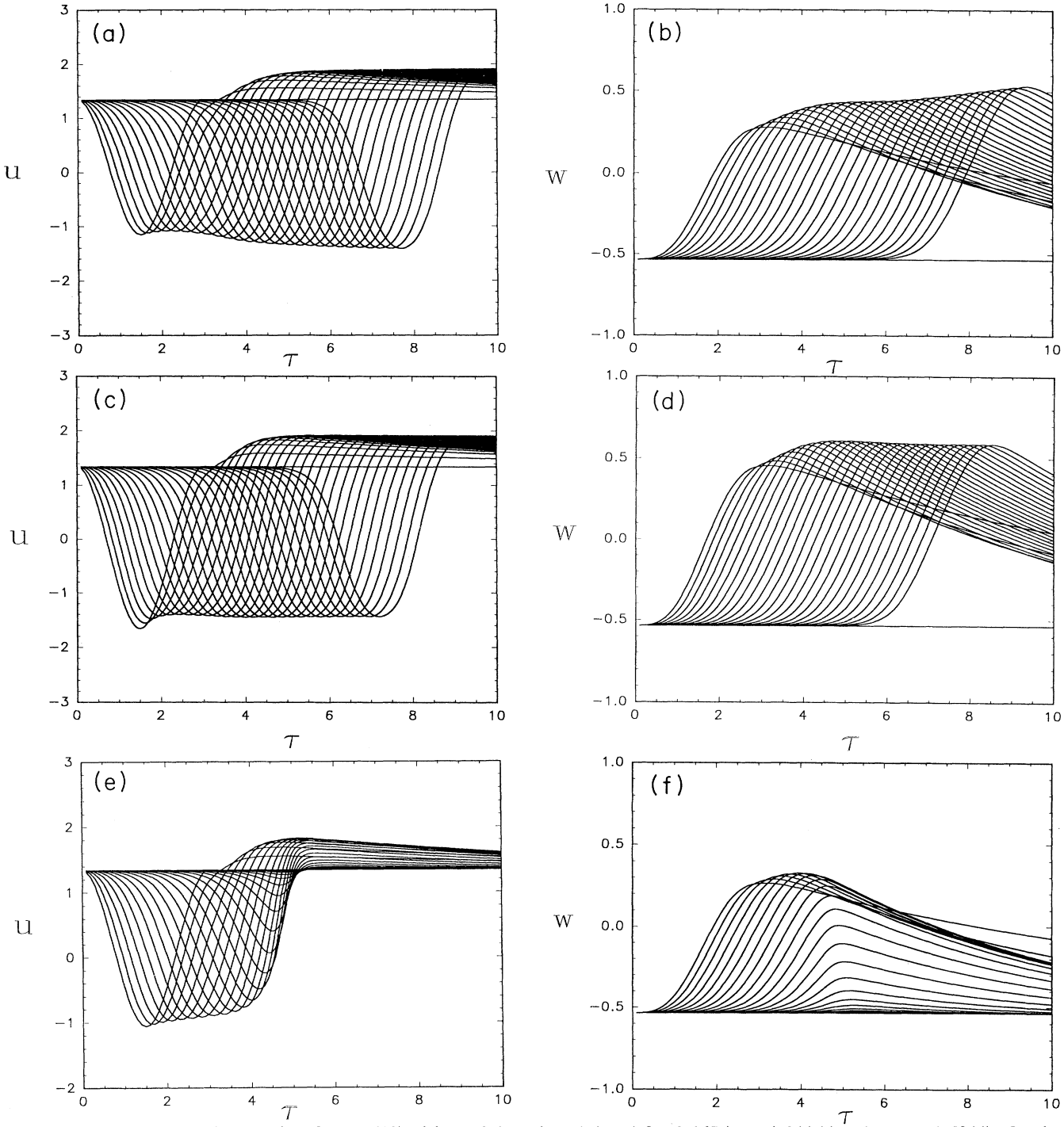

FIG. 8. A boundary-value problem for Eq. (30) with $\mu=3.0$, and $\varepsilon=0.1$ and $\Omega=0.067$ ($u_0=1.344\,44$ and $w_0=-0.5344$). On the line $\tau=0$, $u=u_0$, where $\partial u/\partial\tau=0$. On the line $x=0$, $u=F(\tau)=u_0+H(1-\cos 2\pi\tau/\tau_0)$ for $\tau_0\geq\tau>0$ and $u=u_0$ for $\tau\geq\tau_0$. (a) A signal above the threshold value and below the asymptotic value is amplified during transmission. Graph of u versus τ. (b) A signal above the threshold value and below the asymptotic value is amplified during transmission. Graph of w versus τ. (c) A signal above the asymptotic value is attenuated during transmission. Graph of u versus τ. (d) A signal above the asymptotic value is attenuated during transmission. Graph of w versus τ. (e) A signal below the threshold value is eliminated during transmission. Graph of u versus τ. (f) A signal below the threshold value is eliminated during transmission. Graph of w versus τ. (g) The u-asymptotic wave form versus x corresponding to (c). (h) The w-asymptotic wave form versus x corresponding to (d). (i) For $b_0=0.15$ instead of 0.1, as in (a)–(h), the soliton travels along x, but slowly diminishes. Graph of u versus τ. (j) For $b_0=0.15$ instead of 0.1, as in (a)–(h), the soliton travels along x, but slowly diminishes. Graph of w versus τ. (k) Action potential obtained from the HH equations (cf. Appendix C for the values of the parameters and calculation). Although the resting potential is shown to be 0 mV in the figure, the current convention is to take it as ~ -60 mV, so that the peak is at ~ 40 mV. The oscillating tail or the after potential is not shown.

If the solution of this partial differential equation has a wave form that is transmitted along a line without distortion and with a constant velocity (say c_s), then the solution must be a function of $t' \equiv t - x/c_s$, which is the retarded time. In such a case,

$$\tau' \equiv \tau - \frac{x'}{\sigma_s}, \quad \omega(\tau') = z(x', \tau) ,$$

where

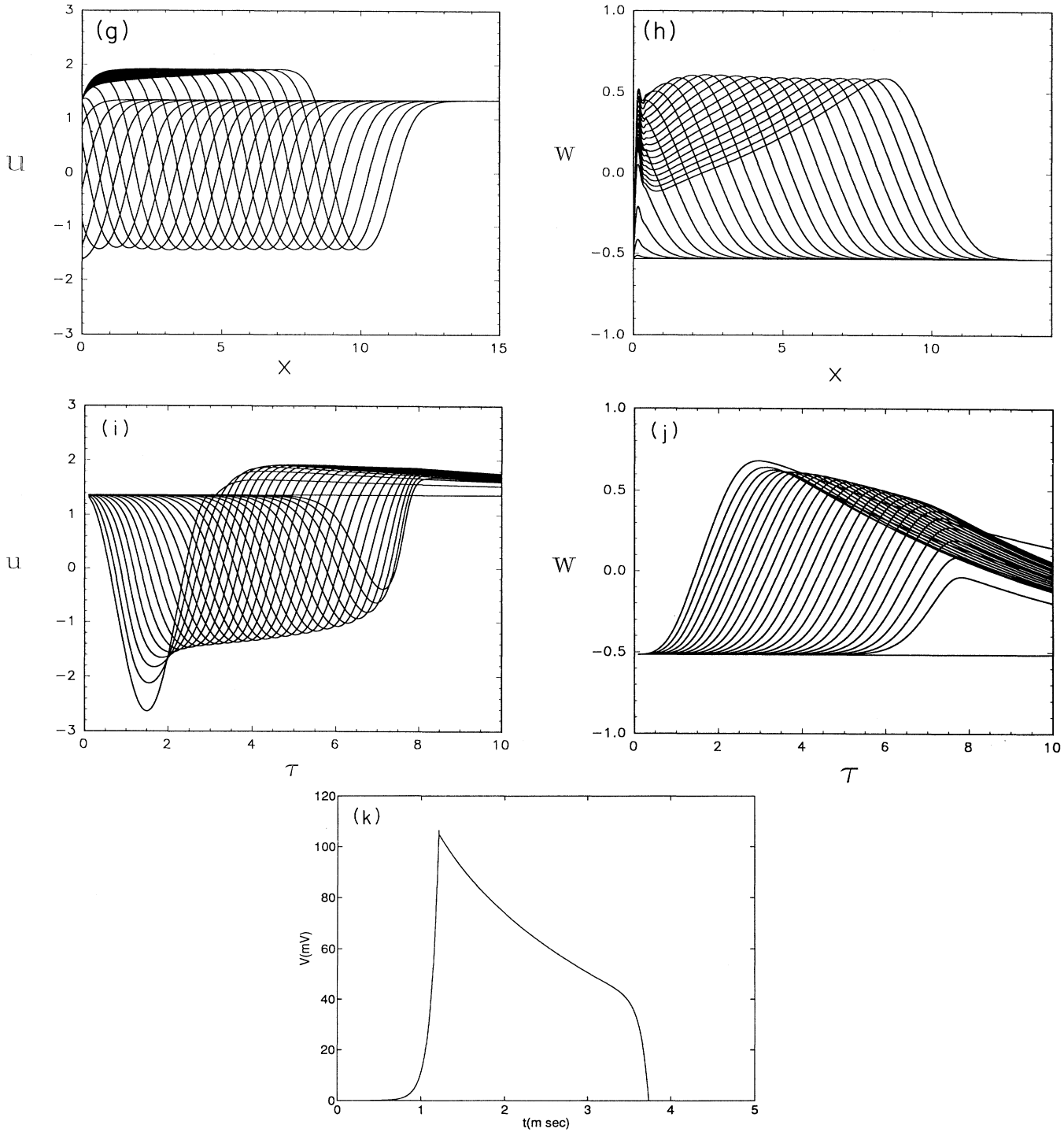

FIG. 8. (*Continued*).

$$\sigma_s^2 \equiv \frac{c_s^2 \gamma}{c_0 h_0 \beta \bar{c}} ,$$

thereby obtaining the ordinary differential equation

$$\frac{1}{\sigma_s^2}\omega''' + \left[\frac{b_0}{c_0\sigma_s^2} - 1\right]\omega'' - \left[\mu(1-\omega+\varepsilon\omega^2) + \frac{b_0}{c_0}\right]\omega' - (1+\Omega)\omega + \frac{1}{2}\Omega\omega^2 - \frac{1}{3}\varepsilon\Omega\omega^3 - (\Omega+b_0)\left[-2+\frac{1}{3\varepsilon}\right] = 0 , \quad (32)$$

where the prime refers to differentiation with respect to τ'. The velocity of the asymptotic wave form is

$$c_s = \left[\frac{c_0 h_0 \beta \bar{c}}{\gamma}\right]^{1/2} \sigma_s(\mu,\varepsilon,\Omega) = (\pi R K_b)^{1/2}\left[\frac{\bar{c}\beta}{\gamma^3}\right]^{1/4} \sigma_s(\mu,\varepsilon,\Omega) , \quad (33)$$

where $\sigma_s(\mu,\varepsilon,\Omega)$ is obtained by solving Eq. (32) numerically.

For the resting solution of Eq. (32), $\omega=\omega_0$, we solve

$$-\frac{1}{3}\Omega\varepsilon\omega_0^3 + \frac{1}{2}\Omega\omega_0^2 - (1+\Omega)\omega_0 - (\Omega+b_0)\left[-2+\frac{1}{3\varepsilon}\right] = 0$$

to obtain $\omega_0 = -0.207\,316\,7$ for $b_0 = 0.1$. In order to obtain an appropriate characteristic equation, we let

$$\omega = \omega_0 + \tilde{\omega} ,$$

thus obtaining

$$\tilde{\beta}\tilde{\omega}''' + \left[\frac{b_0\tilde{\beta}}{c_0} - 1\right]\tilde{\omega}'' - \left[\mu(1-\omega_0+\varepsilon\omega_0^2) + \frac{b_0}{c_0} + \mu(-\tilde{\omega}+\varepsilon\tilde{\omega}^2+2\varepsilon\omega_0\tilde{\omega})\right]\tilde{\omega}' + [\Omega\omega_0 - (1+\Omega) - \Omega\varepsilon\omega_0^2]\tilde{\omega} + \Omega(\tfrac{1}{2}-\varepsilon\omega_0)\tilde{\omega}^2 - \tfrac{1}{3}\Omega\varepsilon\tilde{\omega}^3 = 0 , \quad (34)$$

which has a resting solution $\tilde{\omega}=0$ and the characteristic equation

$$H(\lambda) \equiv \tilde{\beta}\lambda^3 + \left[\frac{b_0\tilde{\beta}}{c_0} - 1\right]\lambda^2 - \left[\mu(1-\omega_0+\varepsilon\omega_0^2) + \frac{b_0}{c_0}\right]\lambda + \Omega\omega_0 - (1+\Omega) - \Omega\varepsilon\omega_0^2 = 0 ,$$

with $\tilde{\beta} = 1/\sigma_s^2$.

We used $a_0 = 1.291$, $b_0 = 0.1$, and $c_0 = 4.5$; this corresponds to $\mu = 3.0$, $\varepsilon = 0.1$, and $\Omega = 0.067$. With $b_0 = 0$, this choice reduces to that of Nagumo, Arimoto, and Yoshizawa [7]. The characteristic equation reduces to

$$H(\lambda) \equiv \tilde{\beta}\lambda^3 + (\tfrac{1}{45}\tilde{\beta} - 1)\lambda^2 - 3.657\,066\lambda - 1.081\,178 = 0 .$$

This equation has a positive real root since $H(0)<0$, $H'(0)<0$, and $H(\infty)>0$. The other two roots are real negative if $\tilde{\beta} < \tilde{\beta}_0(\mu) = 4.213$ for $\mu = 3.0$; otherwise they are complex conjugates with real negative parts. Denoting the positive root by λ_0 (>0),

$$H(\lambda) = (\lambda-\lambda_0)\left\{\tilde{\beta}\lambda^2 + \gamma\lambda - \frac{1}{\lambda_0}[\Omega\omega_0 - (1+\Omega) - \Omega\varepsilon\omega_0^2]\right\} ,$$

where

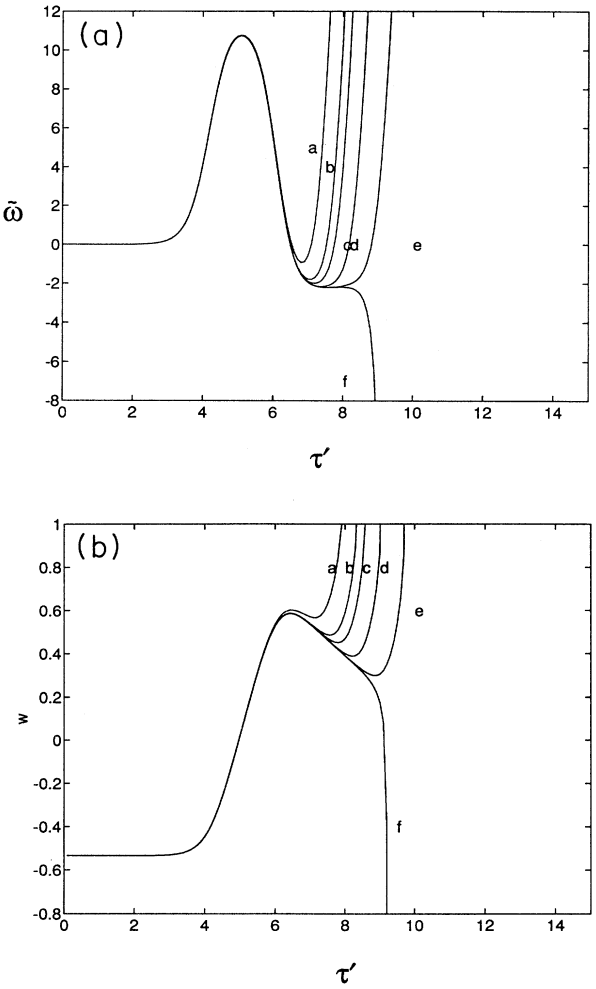

FIG. 9. (a) For $\tilde{\beta} \approx 0.651\,761\,7$, it is expected that a stable asymptotic wave form exists. For this case, $\mu = 3.0$, and $\varepsilon = 0.1$ and $\Omega = 0.067$. Labels on the graph are given as *a*, $\tilde{\beta} = 0.65$; *b*, $\tilde{\beta} = 0.651\,56$; *c*, $\tilde{\beta} = 0.651\,70$; *d*, $\tilde{\beta} = 0.651\,755$; *e*, $\tilde{\beta} = 0.651\,761\,5$; and *f*, $\tilde{\beta} = 0.651\,762$. Note that $\tilde{\beta} = 0.651\,761\,7$ ($b_0 = 0.1$) for our case is larger than the estimate of Nagumo *et al.*: $\tilde{\beta} = 0.444\,88$ ($b_0 = 0.0$). (b) *w*-asymptotic wave form: *a*, $\tilde{\beta} = 0.65$; *b*, $\tilde{\beta} = 0.651\,56$; *c*, $\tilde{\beta} = 0.651\,70$; *d*, $\tilde{\beta} = 0.651\,755$; *e*, $\tilde{\beta} = 0.651\,761\,5$; and *f*, $\tilde{\beta} = 0.651\,762$.

$$\gamma=\tilde{\beta}\lambda_0+\frac{b_0\tilde{\beta}}{c_0}-1=\frac{1}{\lambda_0}\left[3(1-\omega_0+0.1\omega_0^2)+\frac{b_0}{c_0}\right]$$
$$-\frac{1}{\lambda_0^2}[\Omega\omega_0-(1+\Omega)-\Omega\varepsilon\omega_0^2] .$$

Now, if $\tilde{\omega}(\tau')\to 0$ when $\tau'\to-\infty$, then $\tilde{\omega}(\tau')\sim\tilde{A}\exp(\lambda_0\tau')$, where $\tilde{A}$ is an arbitrary constant. Hence

$$\omega'(\tau')\sim\tilde{A}\lambda_0\exp(\lambda_0\tau'),\quad \omega''(\tau')\sim\tilde{A}\lambda_0^2\exp(\lambda_0\tau') .$$

Thus we have performed numerical calculations for the third-order differential equation [Eq. (34)] using the initial conditions

$$\tilde{\omega}(0)=\Delta,\quad \tilde{\omega}'(0)=\lambda_0\Delta,\quad \tilde{\omega}''(0)=\lambda_0^2\Delta ,$$

where Δ (>0) is the smallest step of ω. We are seeking the value for $\tilde{\beta}$ such that $\tilde{\omega}(\tau')\to 0$ when $\tau'\to\infty$, as shown in Fig. 9.

VI. DETERMINATION OF ANISOTROPIC VISCOELASTIC CONSTANTS

Since the speed of the solitary wave depends on the anisotropic viscous and elastic constants of the material, their experimental determination is discussed in the following sections.

A. Elastic constants

Obviously, we need to determine the A set of elastic constants represented by $(\overline{A}_{12}+\overline{A}_{11})$ and $(\overline{A}_{21}+\overline{A}_{11})$ and the B set represented by $(B_{12}+B_{11})$ and $(B_{21}+B_{11})$. A Sm-C^* liquid crystal has a helicoidal twist; however, this can be avoided by using a racemic mixture of the material in a wedge which forms part of the cylinder shown in Fig. 2 such that the director **n** lies in the r-x plane, with **n** making an angle θ with **r**. One can induce a Fréedericksz transition by applying a field along α having a voltage difference $U\geq U_c$ given by [23]

$$\varepsilon_a\varepsilon_0U_c^2=\pi^2\overline{B}_2-2\beta^2[(\overline{A}_{21}+\overline{A}_{11})+(B_{21}+B_{11})\theta^2] ,$$

where ε_a is the dielectric anisotropy, ε_0 is the dielectric constant of a vacuum, and B_2 is given by [23]

$$B_2=\overline{B}_2\theta^2 .$$

$\overline{B}_2$ corresponds to the energy associated with a c-director, which is nonuniform with respect to the smectic layers.

The wedge angle β can be varied, thus allowing the determination of $\overline{B}_2$ and $[(\overline{A}_{21}+\overline{A}_{11})+(B_{21}+B_{11})\theta^2]$. One needs to vary θ in order to obtain separate values for $(\overline{A}_{21}+\overline{A}_{11})$ and $(B_{21}+B_{11})$. This can be achieved by applying a strong electric or magnetic field, preferably the latter, along r (decreasing θ) or x (increasing θ). The electric field along α can be applied simultaneously to obtain the Fréedericksz threshold U_c for this new θ. Changing θ means a change of the layer spacing. The associated elastic energy is very high [see Eq. (7.68) in Ref. [20]]; hence a strong field is required.

In order to obtain the other set of constants, e.g., $(\overline{A}_{12}+\overline{A}_{11})$ and $(B_{12}+B_{11})$, one needs to prepare the sample such that **n** is in the r-α plane and apply an electric field along x, i.e., $\mathbf{E}=E\mathbf{x}$. The Fréedericksz threshold is given by

$$\varepsilon_a\varepsilon_0\langle d\rangle E_c^2=\pi^2\overline{B}_1-2\beta^2(\overline{A}_{12}+\overline{A}_{11}) ,$$

where

$$\langle d\rangle=(R+\delta R/2)$$

is the average sample thickness. $\delta R\ll R$ and the sample is filled between R and $R+\delta R$. In order to determine separate values for $(\overline{A}_{12}+\overline{A}_{11})$ and $(B_{12}+B_{11})$, one again needs to vary θ by applying a constant strong electric or magnetic field along α (increasing θ) or r (decreasing θ).

B. Viscosity coefficient γ

As we already noted, soliton C cannot propagate without an electric field. However, under this condition, solitons A and B can propagate with equal velocities given by

$$c_A=c_B=\frac{3\sqrt{3}}{2\gamma}\left[\frac{\pi bK_bR}{2}\right]^{1/2} .$$

It is possible to use this expression for the determination of γ since the other quantities are measurable by other techniques.

A propagating mechanical soliton can be generated in a Sm-C film held between two plates by a technique such as separating the upper plate into two unequal pieces or using a very small exciter driven by electromagnetic techniques. One may study such a film having a cylindrical symmetry by using an observational technique similar to that described by Zhu [11].

Cladis and van Saarloos [4] prepared a free-standing circular smectic-C film and applied a circular shear by rotating a needle located at the center of the film. With a videocamera and a photodiode, they were able to photograph the solitons in the radial direction and to measure the time constant $\tau=B/\gamma_1$, where B is a Saupe coefficient in the language of de Gennes [20] and γ_1 is an anisotropic viscosity coefficient different from γ.

Hydrodynamic studies of Sm-C phases [37,38] are difficult since both a density wave and orientational ordering (i.e., layer bending and c-director deformations) are involved. Our γ and γ_1 of Cladis and Van Saarloos [4] should be expressible in terms of 13 fundamental viscosities [37].

VII. POLYMORPHISM OF LIPID BILAYERS AND MECHANICOELECTRIC TRANSDUCTION IN MEMBRANES

In this section, we discuss the polymorphism exhibited by lipid bilayers. Our nomenclature follows that used for thermotropic liquid crystals, as pointed out in Sec. I. Smectic phases A and C are observed above the chain melting transition and are often referred to as fluid or liquid crystalline phases [12,39,40]. At low temperature

or high pressure, a fluid membrane undergoes transition to a solidlike smectic-B phase [12,40], characteristic of paraffin-hydrocarbon chains in the all-trans configuration. The lipid molecules exhibit a long-range order within the plane of the membrane. With respect to the layer normal, the hydrocarbon chains may be tilted (type B_C) or untilted (type B_A). The tilted configuration may also exhibit an undulated structure (type B_{CA}).

Some ion channels are known to be stretch activated [41]. A mechanical deformation of the membrane consists of a curvature elasticity term and a membrane tension term. Mechanicoelectric transduction has been known to occur in some cells. For example, local deformation of the lobster [42] and Myxicola [43] giant axons produce a depolarization. The idea is that the curvature strain and/or the membrane stretch affects the ion channels so as to affect the ion transmission. The resulting depolarization of the membrane has an effect on the curvature strain through a ferroelectric coupling. Lipid molecules are chiral [44], i.e., have handedness; thus circumstantial evidence is strong that cell membranes have ferroelectric properties. Cell membranes can have spontaneous electric polarization, i.e., ferroelectricity or curvature-induced electric polarization (flexoelectricity). The net polarization owes its origin to a flexoelectric mechanism, as noted in Sec. III. For ferroelectricity, the lipid molecules needs to be cooperatively tilted with respect to the layer normal. Evidence for this comes from dielectric relaxation experiments [45].

VIII. SOLITON LATTICE

In this section, our intention is to derive the static profile of the tilt angle θ versus the distance in the axial direction x. The analysis shows that cell membranes have a modulated structure, consistent with current models [12].

The stationary condition for F, given by Eq. (17), leads to an Euler-Lagrange equation expressed as

$$\frac{d^2\theta}{dx^2}=a\theta^3-b\theta-c \ , \tag{35}$$

where

$$a\equiv\frac{4}{K_b}\left[\frac{Bd}{R^2}-\frac{4\sigma}{3}\right] ,$$

$$b\equiv\frac{2}{K_b}\left[d\Xi(\xi)\mu_p^2\cos^2\xi-\left[\frac{Ad}{R^2}+4\sigma\right]\right] ,$$

$$c\equiv\frac{d\mu_p E}{K_b}\Xi(\xi)\sin\xi\cos\xi \ .$$

Equation (35) gives the static profile of the membrane structure (θ versus x). First, we consider the simpler case when $c=0$, i.e., the electric field is absent.

The first integration of Eq. (35) gives

$$\left[\frac{d\theta}{dx}\right]^2=\frac{1}{2}a\theta^4-b\theta^2+K_e \ ,$$

where the integration constant K_e is evaluated by using the boundary condition

$$\theta=\theta_0, \quad \frac{d\theta}{dx}=0 \ .$$

Thus $K_e=b\theta_0^2-a\theta_0^4/2$, yielding

$$x-x_0=\int_0^{\theta}\frac{d\theta}{\left[\frac{a}{2}(\theta^4-\theta_0^4)-b(\theta^2-\theta_0^2)\right]^{1/2}} \ ,$$

where x_0 is the position of an arbitrary reference point where $\theta=0$ (see Fig. 10). Substituting $\theta/\theta_0=\sin u'$ gives

$$k'(x-x_0)=\int_0^{\arcsin\theta/\theta_0}\frac{du'}{(1-m^2\sin^2u')^{1/2}} \ ,$$

where

$$k'\equiv\left[\frac{2b-a\theta_0^2}{2}\right]^{1/2} ,$$

$$m^2\equiv\frac{2a\theta_0^2}{2b-a\theta_0^2} ,$$

$$\arcsin\frac{\theta}{\theta_0}=u'=\mathrm{am}\left[\frac{k'(x-x_0)}{m},m\right], \quad 0\le m^2\le 1 \ ,$$

where $\mathrm{am}(u,m)$ is the Jacobi amplitude function. Therefore the solution for θ is given by [31,46,47]

$$\frac{\theta}{\theta_0}=\sin\left[\mathrm{am}\left[\frac{k'(x-x_0)}{m},m\right]\right]=\mathrm{sn}\left[\frac{k'(x-x_0)}{m},m\right] ,$$

where sn is the Jacobi sn function. The half period is given by

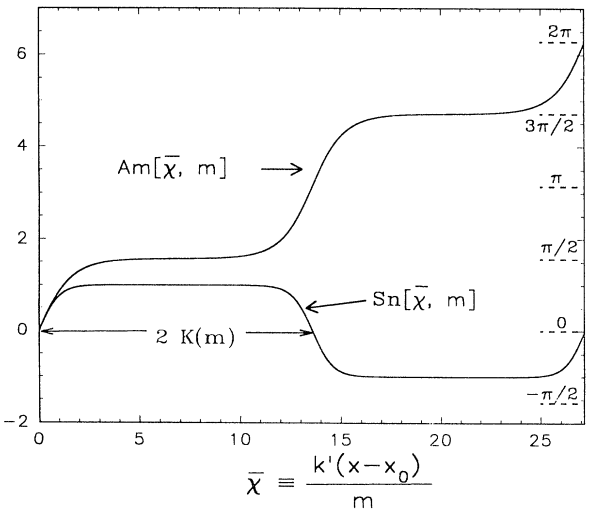

FIG. 10. Soliton lattice of the cell membrane. The competition between piezoelectricity and curvature elasticity produces a tilt angle θ modulation versus distance x along the axial direction. The graph shows $\theta/\theta_0=\mathrm{sn}[k'(x-x_0)/m,m]$ versus $\bar{\chi}=k'(x-x_0)/m$ (see Sec. VIII). The function $\mathrm{am}(\bar{\chi},m)$ is also defined in Sec. VIII.

$$X \equiv \frac{2mK(m)}{\left[\frac{2b-a\theta_0^2}{2}\right]^{1/2}} ,$$

where $K(m)$ is the complete elliptic integral of the first kind. A graph showing the variation of θ/θ_0 with respect to x is given in Fig. 10. When the electric field is on, the problem can be treated by a perturbation technique [47].

Let

$$\theta(x)=\theta_m(x)-\theta'(x) ,$$

where $\theta_m(x)$ is the exact solution for $E=0$ and $-\theta'(x)$ represents the contribution due to the electric field. To first order in $\theta'(x)$ and E we have

$$\frac{d^2\theta'}{dx^2}+\left[-3a\theta_0^2\mathrm{sn}^2\left[\frac{k'x}{m}\right]+b\right]\theta'-c=0 . \tag{36}$$

Let

$$\theta'=\frac{c}{b}+\theta_1' .$$

Then

$$\frac{d^2\theta_1'}{dx^2}+b\theta_1'-\frac{3ac\theta_0^2}{b}\mathrm{sn}^2\left[\frac{k'x}{m}\right] -3a\theta_0^2\theta_1'\mathrm{sn}^2\left[\frac{k'x}{m}\right]=0 , \tag{37}$$

$$\frac{d^2\theta_1'}{dx^2}+\left[b-3a\theta_0^2\mathrm{sn}^2\left[\frac{k'x}{m}\right]\right]\theta_1' =\frac{3ac\theta_0^2}{b}\mathrm{sn}^2\left[\frac{k'x}{m}\right] =\sum_{n=1}^{\infty}\epsilon a_{0,n}\cos\left[\frac{(2n-2)\pi x}{X}\right] ,$$

where

$$a_{0,n}=\frac{2\pi^2}{m^2K^2(m)}\sum_{p=1}^{\infty}\left[\frac{q^{2p-n}}{(1-q^{2p-2n+1})(1-q^{2p-1})} -\frac{q^{n-1}}{(1-q^{2p-1})(1-q^{2n-1-2p})}\right] ,$$

$$\epsilon\equiv\frac{3ac\theta_0^2}{b} ,$$

and the following Fourier expansion has been used:

$$\mathrm{sn}\left[\frac{k'x}{m}\right]=\sin\left[\mathrm{am}\left[\frac{k'x}{m}\right]\right] =\frac{2\pi}{mK(m)}\sum_{n=1}^{\infty}\frac{q^{n-1/2}}{1-q^{2n-1}}\sin\left[(2n-1)\frac{\pi x}{X}\right] ,$$

with

$$q\equiv\exp\left[-\frac{\pi K'(m)}{K(m)}\right], \quad K'(m)\equiv K(\sqrt{1-m^2}) .$$

The solution of Eq. (37) can be written as

$$\theta_1'=\theta_1''+\theta_1''' ,$$

where

$$\frac{d^2\theta_1''}{dx^2}+b\theta_1''=\sum_{n=1}^{\infty}\epsilon a_{0,n}\cos\frac{(2n-2)\pi x}{X} \tag{38}$$

and

$$\frac{d^2\theta_1'''}{dx^2}+b\theta_1'''-3a\theta_0^2\theta_1'''\mathrm{sn}^2\left[\frac{k'x}{m}\right]=3a\theta_0^2\theta_1''\mathrm{sn}^2\left[\frac{k'x}{m}\right] . \tag{39}$$

The solution of Eq. (38) is

$$\theta_1''=\sum_{n=1}^{\infty}\frac{\frac{\epsilon a_{0,n}}{b}\left[\cos\frac{(2n-2)\pi x}{X}\right]}{\left[1-\left[\frac{\xi_0(2n-2)\pi}{X}\right]^2\right]} \quad \text{with } \xi_0^2\equiv\frac{1}{b} ,$$

while the second member of Eq. (39) can be developed to give an equation for θ_1''' formally identical to Eq. (37):

$$\frac{d^2\theta_1'''}{dx^2}+b\theta_1'''-3a\theta_0^2\theta_1'''\mathrm{sn}^2\left[\frac{k'x}{m}\right] =\sum_{n=1}^{\infty}\epsilon a_{1,n}\cos\frac{(2n-2)\pi x}{X} ,$$

with $(i=0)$

$$a_{i+1,n}=\frac{3a}{b}\sum_{p=1}^{\infty}\frac{(a_{i,n-p+1}+a_{i,n+p-1})a_{i,p}}{\left[1-\frac{\xi_0^2(2p-2)^2\pi^2}{X^2}\right]} .$$

Iterating the process leads to an exact, although complicated, solution of Eq. (36):

$$\theta'=\frac{c}{b}+\frac{\epsilon}{b}\sum_{i=0}^{\infty}u_n\cos\frac{(2n-2)\pi x}{X} ,$$

where

$$u_n=\sum_{n=1}^{\infty}\frac{a_{i,n}}{1-\left[\frac{\xi_0(2n-2)\pi}{X}\right]^2} .$$

This result modifies, to some extent, the θ versus x variation shown in Fig. 10, which is valid for the case in which the electric field is absent. Even in the presence of the electric field, the θ versus x variation remains periodic with the same period as that for $E=0$, although the dc level is shifted. Depending on the sign of the field, one of the two types of regions θ or $-\theta$ expands and the other shrinks. This situation holds as long as the electric field is not too high for the perturbation scheme to break

down. For very high electric fields, the tilt angle modulation along the axial direction x should vanish.

IX. CONCLUDING REMARKS

In the usual Sm-C^* geometry considered by various authors [4], the electric field is applied along the y direction in the layer plane (see Fig. 1), and if there is no head-to-tail correlation of the molecules, the component of the electric polarization normal to the transverse polarization direction is completely disordered. The Lifshitz term and the piezoelectric and the flexoelectric terms in the free energy ensure a helicoidal twist along the z axis. The c director rotates as one travels along the helix axis and so does the electric polarization vector, which is perpendicular to the c director in the layer plane. The soliton equation in this case, given by Eq. (1), shows the azimuthal angle ϕ as the independent variable.

The mechanism of propagation of the solitary wave, also known as ferroelectric switching, depends on the fact that those parts of the helix where the polarization is locally parallel to the field expand and the regions with polarization antiparallel to the electric field shrink. If the field is suddenly reversed, as in the case of an ac or oscillating electric field, the antiparallel regions become parallel regions and a solitary wave propagates as the stable regions grow at the expense of the unstable regions [4].

In a head-to-tail correlated Sm-C^* liquid crystal, the normal component of the electric dipole moment (see Fig. 4) is ordered leading to a longitudinal polarization $\mathbf{p}_r$, which is available for coupling to an electric field existing across the 2D liquid crystal film, e.g., a cell membrane. This electric dipole polarization is in addition to the alignment of transverse steric dipoles characteristic of chiral molecules. The soliton equation for this case, given by Eq. (19), shows the tilt angle θ as the independent variable.

Tilt angle is the "hard" variable; its fluctuation range is small relative to the azimuthal angle. The balance between the curvature elastic energy and the piezoelectric energy produces a modulated structure, which spans the entire membrane space. These modulations consist of juxtaposed regions of opposite tilt orientations. Such a portrayal of the cell membrane is consistent with the current models [12]. The θ and $-\theta$ tilt membrane regions are associated with opposite signs of the longitudinal polarization $\mathbf{p}_r$ and the steric dipole polarization $\mathbf{p}_s$.

The excitable membrane has mainly three types of ions, e.g., K^+, Cl^-, and Na^+, on both the intracellular and the extracellular sides. Chloride ion movement is not considered to be relevant to membrane excitability [35]. The nerve membrane has two steady states. One of these is called the resting state whose potential is governed by the potassium Nernst potential. Under the resting condition, potassium permeability is large and the sodium permeability is very small: $P_K:P_{Na}=1:0.04$ [35]. The resting membrane potential is given by

$$E_K=\frac{RT}{F}\ln\frac{[K^+]_e}{[K^+]_i} .$$

This value is about -60 mV. A mechanical or electrical perturbation changes the tilt angle θ, thus increasing the sodium permeability. The membrane potential increases, becomes zero, and then rises to $+40$ mV, which is about the sodium Nernst potential. This is the other steady state:

$$E_{Na}=\frac{RT}{F}\ln\frac{[Na^+]_e}{[Na^+]_i}, \quad P_K:P_{Na}=1:10$$

(see [35]). The return to the resting state is achieved by potassium efflux from the intracellular to the extracellular region, together with active transport initiated by pumps. These ion pumps restore the transmembrane electrochemical gradient, the energy being derived from metabolism.

If the electric field E changes sign as, for example, happens in nerve membranes [see Fig. 11(a)], the tilt angle θ switches to $-\theta$. This implies the propagation of a solitary wave by ferroelectric switching since there are juxtaposed membrane regions with the tilt angles θ and $-\theta$ [see Fig. 11(b)], which are associated with opposite signs of longitudinal polarization ($\mathbf{p}_r$). If there is no transmembrane dipolar coupling, each monolayer half would have to support a polarization modulation along the axial direction in order that a solitary electrical wave form may propagate. This is not an energetically feasible situation since, in order to have opposite polarization for part of the axial distance, the nonpolar tails would have to face the polar aqueous environment. Thus our equations of motion would be invalid if there is no transmembrane dipolar coupling.

The form for our w or E soliton [see Fig. 8(d)] matches quite well the triangular action potential, which shows fast upstroke and much slower recovery [1]. The Fitzhugh-Nagumo equations interpret u as the membrane potential and as such simulate the threshold behavior of the nerve membrane, but cannot reproduce its recovery properties. The FN equations were derived by reducing the four-dimensional Hodgkin-Huxley equations to the two-dimensional V-m system, where the h and n processes have been characterized as slow and given their steady-state values. In our model, the mechanical variable θ and the transmembrane electric field E appear as the fast and slow variables, respectively. It is conceptually possible to have a cell membrane working on this principle. A cell membrane of this type would show sensitivity towards mechanical stretch and hence can be called a stretch-activated membrane. On the other hand, squid-axon-type cell membranes show sensitivity towards electrical stimulus, as explained in the introductory remarks. Thus, starting from different physical assumptions, our work shows that a two-dimensional model is capable of exhibiting the same kind of excitable-oscillatory behavior as well as propagating solitary-wave-like behavior as the 4D HH model.

The Hodgkin-Huxley model details the electrophysiology of the nerve membrane of the squid axon. There are misgivings regarding the universal applicability of the HH model since the presence of cell membranes in other species which may not obey the HH model cannot be ruled out. At the present time, no other detailed work in

the same spirit as that of Hodgkin and Huxley is available, and we speculate that there may be differences in the electrophysiology of stretch-activated membranes referred to in Sec. VII and other membranes of the squid-axon-type studied by Hodgkin and Huxley. Stretch-activated membranes are those where mechanical deformation affects ion transmission, thus causing membrane depolarization. Our model may be more readily applicable to this stretch-activated variety. However, the form for the action potential in both cases appear similar (cf. Figs. 8 and 9), which, we believe, is due to the presence (in all cell membranes) of a strong electromechanical coupling, the nature of which we have attempted to reveal in the present work through a ferroelectric liquid crystal model, together with a mechanism of transmembrane potential variation.

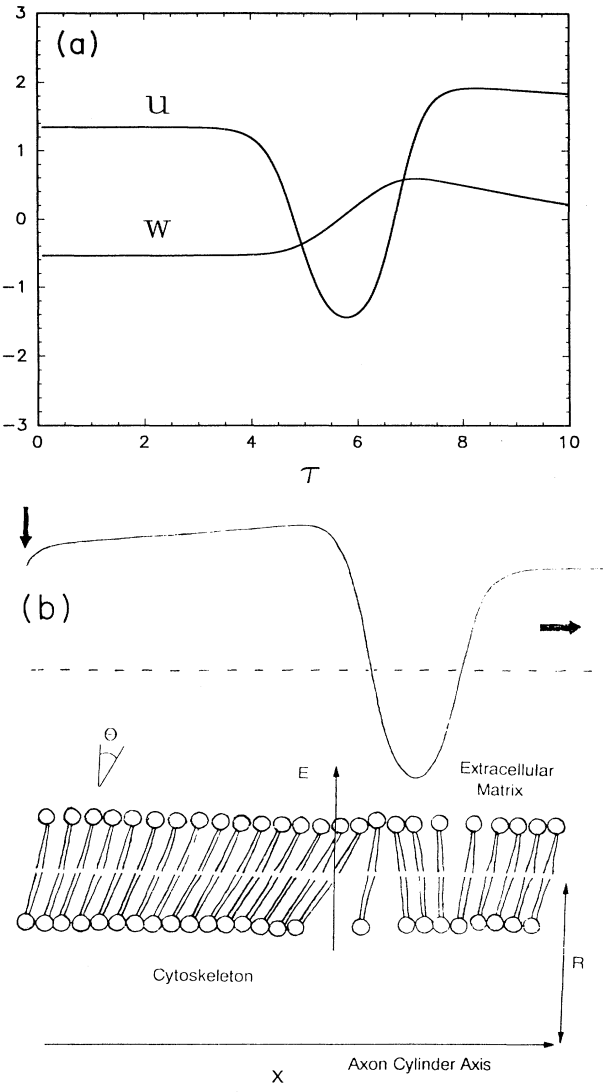

FIG. 11. (a) u and w solitons versus τ. $a_0=1.291$, $b_0=0.1$, $c_0=9/2$, and $h_0=1/c_0$. (b) Schematic showing which lipid molecular reorientations in a cell membrane constitute the solitary wave form displayed above the membrane. The arrow at the top left shows the location where the membrane is imparted a stimulus which, as function of time, approaches the asymptotic soliton shape [Fig. 8(g)]. The solitary wave shown here corresponds to a profile of the molecular tilt angle θ versus the distance in the axial direction x for a long enough time. The dashed line stands for $\theta=0$. E is the magnitude of the electric field whose sign is indicated by the trans-bi-layer arrow.

Another important point is the effect of the parameter b_0 in Eq. (30). Solitons for $b_0=0$ and 0.1 have almost the same width and amplitude, but solitons do not exist for $b_0=0.15$. Since b_0 depends upon electrical and mechanical parameters, it is conceptually possible to test this prediction experimentally.

Another kind of nerve propagation which should be mentioned in this context is myelinated nerve conduction. The myelin sheath consists of about 100 stacked cell membranes with no imbedded proteins. Because of the thick lipid coating and the absence of transport proteins, no ion transmission can occur and the transmembrane electric field remains static and cannot be oscillatory. The propagating action potential does not have the benefit of regeneration while in the myelin sheath and gets considerably distorted in shape and size as it emerges at the node of Ranvier where regeneration occurs. The regenerated action potential then resumes its journey through the next myelin sheath [35].

Because of the radial extension of the system, the static and dynamical equations are more complicated, since in addition to the cylindrical axis, and radial coordinate is needed. The saltatory myelinated conduction and the solitary-wave-like unmyelinated conduction compliment each other in significant ways, so that important insight into cellular processes can be obtained from their studies.

We call our model "molecular" because the elastic [48] and viscometric constants [49] are expressible in terms of molecular parameters such as length, diameter, volume fraction of the lipid rods, and the relevant order parameter; the piezoelectric coefficient (see Sec. III) is expressible in terms of molecular parameters; the membrane capacitance can be related to its dielectric constant for which molecular theories exist [50]. We have attempted in this work to construct a model of the nerve membrane from which, by the use of physical laws, the mechanical, chemical, and electrical properties of the membrane can be derived. To our knowledge, advances in the area of nerve excitability, apart from the seminal experimental work of Hodgkin and Huxley, has so far been restricted to the development of purely mathematical models such as those of Fitzhugh and Nagumo and Hodgkin and Huxley. The mathematical theory of nerve conduction was mostly developed several decades ago [1,6,7]. It is conceptually useful to construct different mathematical models which emphasize one or another set of properties and omit others. Clearly, the next step in the development is to combine both physical and mathematical descriptions to base the model on the laws of physics and chemistry. Such an attempt has been made in this work, and hopefully better insight will be forthcoming in the future in this (i.e., solitary-wave-like) and other (i.e., periodic train of waves) aspects of nerve conduction.

ACKNOWLEDGMENTS

P.D. wishes to gratefully acknowledge the support obtained from the NSF Biological Research Center Grant No. DIR-8721059. We also thank Matthew Fisher for his assistance with the diagrams.

APPENDIX A

Equation (20) has three solutions: solitons A, B, and C. The velocity and half-width of soliton C have been recorded in Sec. IV, while those of solitons A and B are given below.

For soliton A

$$\theta_A = \left[\frac{b}{a}\right]^{1/2} [\cos\theta_0 - \cos(\theta_0 + \tfrac{4}{3}\pi)]\{1 - \tanh[W_A^{-1}(X - X_0 - C_A T)]\} + \left[\frac{b}{a}\right]^{1/2} \cos(\theta_0 + 4\pi/3)$$
$$= \left[\frac{3b}{a}\right]^{1/2} \sin(\theta_0 + 2\pi/3)\{1 - \tanh[W_A^{-1}(X - X_0 - C_A T)]\} + \left[\frac{b}{a}\right]^{1/2} \cos(\theta_0 + 4\pi/3) ,$$

where the width of the soliton wave is given by

$$W_A = \left[\frac{2}{3}\right]^{1/2} \left[\left[\frac{b}{a}\right]^{1/2} \sin(\theta_0 + 2\pi/3)\right]^{-1} .$$

In dimensional units,

$$w_A = \left[\frac{\pi RK}{a}\right]^{1/2} \left[\left[\frac{b}{a}\right]^{1/2} \sin(\theta_0 + 2\pi/3)\right]^{-1} .$$

The wave speed is

$$C_A = 3\left[\frac{b}{2a}\right]^{1/2} \cos\left[\frac{\pi}{3} - \theta_0\right] .$$

In dimensional units,

$$c_A = \left[\frac{\pi RK}{a}\right]^{1/2} \frac{3a}{\gamma\sqrt{2}} \left[\frac{b}{a}\right]^{1/2} \cos\left[\frac{\pi}{3} - \theta_0\right] . \tag{A1}$$

For $c = 0$, $\theta_0 = \pi/6$ and $\cos(\pi/3 - \theta_0) = \sqrt{3}/2$. Thus Taylor expanding near $\theta_0 = \pi/6$ and retaining terms to first order in c/c_0 gives

$$c_A \approx \frac{3\sqrt{2}}{2\gamma} \left[\frac{\pi b R K_b}{2}\right]^{1/2} \left[1 - \frac{c a^{1/2}}{2b^{3/2}}\right] .$$

For soliton B

$$\theta_B = \left[\frac{b}{a}\right]^{1/2} [\cos(\theta_0 + 4\pi/3) - \cos(\theta_0 + 2\pi/3)]\{1 - \tanh[W_B^{-1}(X - X_0 - C_B T)]\} + \left[\frac{b}{a}\right]^{1/2} \cos(\theta_0 + 2\pi/3)$$
$$= \left[\frac{3b}{a}\right]^{1/2} \sin\theta_0\{1 - \tanh[W_B^{-1}(X - X_0 - C_B T)]\} + \left[\frac{b}{a}\right]^{1/2} \cos(\theta_0 + 2\pi/3) ,$$

where the dimensionless width is given by

$$W_B = \left[\frac{2}{3}\right]^{1/2} \left[\left[\frac{b}{a}\right]^{1/2} \sin\theta_0\right]^{-1} .$$

In dimensional terms

$$w_B = \left[\frac{\pi RK}{a}\right]^{1/2} \left[\left[\frac{b}{a}\right]^{1/2} \sin\theta_0\right]^{-1} .$$

The dimensionless wave speed is

$$C_B = 3\left[\frac{b}{2a}\right]^{1/2} \cos\phi_0$$

and in dimensional terms

$$c_B = 3\left[\frac{\pi RK}{2a}\right]^{1/2} \frac{a}{\gamma} \left[\frac{b}{a}\right]^{1/2} \cos\theta_0 . \tag{A2}$$

A Taylor expansion about $\theta_0 = \pi/6$ obtains

$$c_B \approx \frac{3\sqrt{3}}{2\gamma}\left[\frac{\pi b R K_b}{2}\right]^{1/2}\left[1+\frac{c a^{1/2}}{2b^{3/2}}\right] .$$

APPENDIX B

We have added the term

$$-\pi R \int dx\, I\left[\frac{d\theta}{dt}\right]^2$$

to the right-hand side of Eq. (17) to account for the rotational kinetic energy, thus defining the negative Lagrangian density

$$\gamma\frac{\partial\theta}{\partial t}=\pi R K_b\frac{\partial^2\theta}{\partial x^2}-2\pi R I\frac{\partial^2\theta}{\partial t^2}-(a\theta^3-b\theta-c) .$$

With rearrangement and redefining of variables, this equation can be cast into the form

$$\theta_{xx}-\theta_{tt}-\lambda\theta_t-(\theta-\theta_1)(\theta-\theta_2)(\theta-\theta_3)=0 .$$

This is the equation of a solitary wave [33] with the half-width

$$a=\frac{1}{\sqrt{2}}(\theta_3-\theta_1)[1+(\theta_3+\theta_1-2\theta_2)^2/(2\lambda^2)]^{1/2}$$

and velocity

$$c=\frac{1}{\sqrt{2}}(\theta_3+\theta_1-2\theta_2)[\lambda^2+\tfrac{1}{2}(\theta_3+\theta_1-2\theta_2)]^{1/2} .$$

APPENDIX C

The Hodgkin-Huxley model [1] views the total transmembrane current I_m as made up of a capacity current $C_0 dV_m/dt$ and ionic currents due to the movement of sodium (Na), potassium (K), and other ions (L):

$$\begin{aligned} I_m &= I_C+I_{\mathrm{Na}}+I_{\mathrm{K}}+I_L \\ &= C_0\frac{dV_m}{dt}+g_{\mathrm{Na}}(V_m-E_{\mathrm{Na}}) \\ &\quad +g_{\mathrm{K}}(V_m-E_{\mathrm{K}})+g_L(V_m-E_L) , \end{aligned}$$

where V_m is the voltage difference between the inside and the outside of the membrane and the g's are the conductances given by

$$g_{\mathrm{Na}}=\bar{g}_{\mathrm{Na}}m^3h,\quad g_{\mathrm{K}}=\bar{g}_{\mathrm{K}}n^4,\quad g_L=\bar{g}_L . \tag{C1}$$

Here m is the sodium activation (dimensionless), h is the dimensionless sodium inactivation, and n is the dimensionless potassium activation, each varying between 0 and 1. The behavior of these quantities is described by [1]

$$\begin{aligned} &\frac{dm}{dt}+[\alpha_m(V_m)+\beta_m(V_m)]m=\alpha_m(V_m) , \\ &\frac{dh}{dt}+[\alpha_h(V_m)+\beta_h(V_m)]h=\alpha_h(V_m) , \\ &\frac{dn}{dt}+[\alpha_n(V_m)+\beta_n(V_m)]n=\alpha_n(V_m) , \end{aligned} \tag{C2}$$

where

$$\begin{aligned} &\alpha_m(V_m)=0.1(V_m+25)\left[\exp\left[\frac{V_m+25}{10}\right]-1\right]^{-1} , \\ &\beta_m(V_m)=4\exp(V_m/18) , \\ &\alpha_h(V_m)=0.07\exp(V_m/20) , \\ &\beta_h(V_m)=1/\{[(V_m+30)/10]-1\} , \\ &\alpha_n(V_m)=0.01(V_m+10)\left[\exp\left[\frac{V_m+10}{10}\right]-1\right]^{-1} , \\ &\beta_n(V_m)=0.125\exp(V_m/80) , \end{aligned} \tag{C3}$$

and V_m is the membrane voltage in millivolts.

Here $C_0=1$ μf/cm^2, $\bar{g}_{\mathrm{Na}}=120$, $\bar{g}_{\mathrm{K}}=36$, $\bar{g}_L=0.3$ mΩ^{-1}cm^{-2}, $E_{\mathrm{Na}}=-115$, $E_{\mathrm{K}}=12$, $E_L=-10.5989$ mV, $R=0.0238$ cm, and $\tilde{R}_i=34.5$ Ω-cm. These values have been used for computation of the phase-plane diagram [Fig. 6(b)] and the action potential [see Fig. 8(k)] for the HH equations.

Solution of Eq. (28) for the form of the HH action potential

The long-time solutions for Eqs. (28) and (C2) are

$$\begin{aligned} &120m_e^3h_e(V_e+115)+36n_e^4(V_e-12) \\ &\qquad +0.3(V_e+10.5989)=0 , \end{aligned} \tag{C4}$$

where

$$\begin{aligned} m_e &= \frac{\alpha_m(V_e)}{\alpha_m(V_e)+\beta_m(V_e)} , \\ h_e &= \frac{\alpha_h(V_e)}{\alpha_h(V_e)+\beta_h(V_e)} , \\ n_e &= \frac{\alpha_n(V_e)}{\alpha_h(V_e)+\beta_n(V_e)} . \end{aligned}$$

The α's and β's are given by Eq. (C3) with $V_m=V_e$ (the resting value of the membrane potential). Equation (C4) can be solved for the resting values V_e, m_e, n_e, and h_e. The behavior near the resting point is described approximately by a linear differential equation

$$\beta_{\mathrm{HH}}\frac{\partial^2\bar{V}}{\partial t^2}-\frac{2\tilde{R}_i C_0}{R}\frac{\partial\bar{V}}{\partial t}=(\bar{g}_{\mathrm{Na}}m_e^3h_e+\bar{g}_{\mathrm{K}}n_e^4+\bar{g}_L)\bar{V} ,$$

where $V_m=\bar{V}+V_0$, $\beta_{\mathrm{HH}}\equiv 1/c_{\mathrm{HH}}^2$ (c_{HH} is the speed of the Hodgkin-Huxley action potential), and

$$V_0=\frac{\bar{g}_{\mathrm{Na}}m_e^3h_eE_{\mathrm{Na}}+\bar{g}_{\mathrm{K}}n_e^4E_{\mathrm{K}}+\bar{g}_LE_L}{\bar{g}_{\mathrm{Na}}m_e^3h_e+\bar{g}_{\mathrm{K}}n_e^4+\bar{g}_L}\approx 0 .$$

Solving Eq. (C4) one obtains $V_e=0$, $m_e=0.052\,93$, $h_e=0.596\,12$, and $n_e=0.317\,677$. The characteristic equation is given by

$$\beta_{\mathrm{HH}}x^2-2.899\,15x-1.963\,461=0 .$$

One of the roots is positive; the other is negative. Denot-

ing the positive root by x_0, it can be easily shown, as in Sec. V B, that the initial conditions on V_m should be $V_m(0)=\Delta$ and $V_m'(0)=x_0\Delta$, where, as in Sec. V B, Δ is the smallest step size. The calculated action potential is shown in Fig. 8(k). These initial conditions together with the equilibrium values for n, h, and m given above obtain the left-hand side of the action potential curve. In order to get the right-hand side of the curve, we used the initial conditions appropriate to the peak of the curve, namely, $V_m(\text{peak})=105$ mV, $m(\text{peak})=0$, $n(\text{peak})=0.3$, and $h(\text{peak})=0.675$. Calculations were carried out for each initial guess of dV/dt. Our calculated value for the wave speed $c_{\text{HH}}=1.881\,264\,53$ m/s is in agreement with the reported value of 1.88 m/s, obtained by a different numerical scheme [1]. $dV/dt=-55.303\,386\,717$ is the value used for Fig. 8(k).

[1] A. L. Hodgkin and A. F. Huxley, J. Physiol. **117**, 500 (1952).
[2] S. J. Singer and G. L. Nicolson, Science **175**, 720 (1972).
[3] M. Edidin, Annu. Rev. Biophys. Bioeng. **3**, 179 (1974).
[4] P. E. Cladis and W. Van Saarloos, in *Solitons in Liquid Crystals,* edited by L. Lam and J. Prost (Springer-Verlag, Berlin, 1992), pp. 116, 134, 138.
[5] G. W. Gray and J. W. Goodby, *Smectic Liquid Crystals Textures and Structures* (Leonard-Hill, Glasgow, 1984).
[6] R. Fitzhugh, Biophys. J **1**, 445 (1961).
[7] J. Nagumo, S. Arimoto, and S. Yoshizawa, Proc. IRE **47**, 2061 (1962).
[8] X. Y. Wang, Phys. Lett. **112A**, 402 (1985).
[9] N. M. Chao and S. H. White, Mol. Cryst. Liq. Cryst. **88**, 127 (1982).
[10] J. L. Ferguson and G. H. Brown, J. Am. Oil Chem. Soc. **49**, 120 (1968).
[11] G. Zhu, Phys. Rev. Lett. **49**, 1332 (1982).
[12] C. Gebhardt, H. Gruler, and E. Sackmann, Z. Naturforsch. C **32**, 581 (1977).
[13] O. G. Mouritsen, in *Physics in Living Matter,* edited by D. Baeriswyl, M. Droz, A. Malaspinas, and P. Martinoli, Lecture Notes in Physics Vol. 284 (Springer-Verlag, Berlin, 1986).
[14] J. E. Maclennan, N. A. Clark, and M. A. Handschy, in *Solitons in Liquid Crystals* (Ref. [4]), p. 153.
[15] J. W. Goodby, in *Ferroelectric Liquid Crystals: Principles, Properties and Applications,* edited by J. W. Goodby, R. Blinc, N. A. Clark, S. T. Lagerwall, M. A. Osipov, S. A. Sakurai, K. Yoshino, and B. Žekš (Gordon and Breach, New York, 1991).
[16] M. Kleman, *Points, Lines, and Walls* (Wiley, New York, 1983), p. 119.
[17] M. D. Mitov, J. F. Faucon, P. Meleard, and P. Bothorel, Adv. Supramole. Chem. **2**, 93 (1992).
[18] P. G. de Gennes, C. R. Acad. Sci. B **275**, 549 (1972).
[19] F. Brochard and J. F. Lennon, J. Phys. (Paris) **11**, 1035 (1975).
[20] P. G. de Gennes, *The Physics of Liquid Crystals* (Clarendon, Oxford, 1975).
[21] S. A. Pikin and M. A. Osipov, in *Ferroelectric Liquid Crystals: Principles, Properties and Applications* (Ref. [15]).
[22] T. Carlsson, I. W. Stewart, and F. M. Leslie, Liq. Cryst. **11**, 49 (1992).
[23] T. Carlsson, I. W. Stewart, and F. M. Leslie, Liq. Cryst. **9**, 661 (1991).
[24] E. Sackmann, in *Light-Induced Charge Separation in Biology and Chemistry,* edited by H. Gerischer and J. J. Katz (Dahlen Konferenzen, Berlin, 1974), pp. 259–285.
[25] E. Sackmann, in *Biological Membranes,* edited by D. Chapman (Academic, New York, 1984), Vol. 5.
[26] A. G. Petrov, *Physical and Chemical Bases of Biological Information Transfer* (Plenum, New York, 1975), p. 111.
[27] A. G. Petrov and Y. V. Pavloff, J. Phys. (Paris) **40**, 455 (1979).
[28] J. Charvolin, P. Manneville, and B. Deloche, Chem. Phys. Lett. **23**, 345 (1973).
[29] J. Seelig and W. Niederberger, Biochemistry **13**, 1585 (1974).
[30] S. A. Pikin and V. L. Indenbom, Usp. Fiz. Nauk **125**, 251 (1978) [Sov. Phys. Usp. **21**, 487 (1978)].
[31] M. Yamashita, in *Solitons in Liquid Crystals* (Ref. [4]), p. 300.
[32] J. Prost and P. Barois, J. Chim. Phys. **80**, 65 (1983).
[33] L. Lam, in *Solitons in Liquid Crystals* (Ref. [4]), p. 20.
[34] P. E. Cladis, H. R. Brand, and P. L. Finn, Phys. Rev. A **28**, 512 (1983).
[35] R. Plonsey and R. C. Barr, *Bioelectricity* (Plenum, New York, 1988).
[36] A. V. Holden, in *Biomathematics,* edited by L. M. Ricciardi and A. C. Scott (North-Holland, Amsterdam, 1982).
[37] P. C. Martin, O. Parodi, and P. S. Pershan, Phys. Rev. A **6**, 2401 (1972).
[38] H. R. Brand and H. Pleiner, J. Phys. (Paris) **41**, 533 (1980).
[39] E. Sackman and H. Träuble, J. Am. Chem. Soc. **94**, 4482 (1972).
[40] R. Lipowsky, Nature **349**, 475 (1991).
[41] F. Guharay and F. Sachs, J. Physiol. **352**, 685 (1984).
[42] F. J. Julian and D. E. Goldman, J. Gen. Physiol. **46**, 297 (1962).
[43] G. Ganot, B. S. Wong, L. Binstock, and G. Ehrenstein, Biochim. Biophys. Acta **649**, 487 (1981).
[44] R. M. Weis and H. M. McConnell, Nature (London) **310**, 47 (1984).
[45] U. Kaatze, R. Henze, and R. Pottel, Chem. Phys. Lipids **25**, 149 (1979).
[46] *Handbook of Mathematical Functions,* Natl. Bur. Stand. Appl. Math. Ser. No. 55, edited by M. Abramowitz and I. A. Stegun (U.S. GPO, Washington, DC, 1964).
[47] P. Barois, J. Pommier, and J. Prost, in *Solitons in Liquid Crystals* (Ref. [4]), p. 199.
[48] J. P. Straley, Phys. Rev. A **8**, 2181 (1973).
[49] G. Marucci, Mol. Cryst. Liq. Cryst. **72**, 153 (1982).
[50] S. Chandrasekhar, *Liquid Crystals* (Cambridge University Press, Cambridge, 1992).